Lifespan prolonging mechanisms and insulin upregulation without fat accumulation in long-lived reproductives of a higher termite

Sarah Séité[1, 2#], Mark C. Harrison[3#], David Sillam-Dussès[4], Roland Lupoli[1, 2], Tom J. M. Van Dooren[5, 6], Alain Robert[4], Laure-Anne Poissonnier[7], Arnaud Lemainque[8], David Renault[9, 10], Sébastien Acket[11], Muriel Andrieu[12], José Viscarra[13], Hei Sook Sul[13], Z. Wilhelm de Beer[7], Erich Bornberg-Bauer[3] and Mireille Vasseur-Cognet[1, 2, 14*]

1- UMR IRD 242, UPEC, CNRS 7618, UPMC 113, INRAe 1392, Paris 7 113, Institute of Ecology and Environmental Sciences of Paris, Bondy, France.

2- University of Paris-Est, Créteil, France.

3- Institute for Evolution and Biodiversity, University of Münster, Münster, Germany.

4- University Sorbonne Paris Nord, Laboratory of Experimental and Comparative Ethology UR4443, Villetaneuse, France.

5- UMR UPMC 113, IRD 242, UPEC, CNRS 7618, INRA 1392, PARIS 7 113, Institute of Ecology and Environmental Sciences of Paris, Paris, France.

6- Naturalis Biodiversity Center, Leiden The Netherlands.

7- Department of Biochemistry, Genetics and Microbiology, Forestry and Agricultural Biotechnology Institute, University of Pretoria, Pretoria, South Africa.

8- Genoscope, François-Jacob Institute of Biology, Alternative Energies and Atomic Energy Commission, University of Paris-Saclay, Evry, France.

9- University of Rennes, CNRS, ECOBIO (Ecosystems, biodiversity, evolution) - UMR 6553, Rennes, France.

10- University Institute of France, Paris, France

11- University of Technology of Compiègne, UPJV, UMR CNRS 7025, Enzyme and Cell

26 Engineering, Royallieu research Center, Compiègne, France.

27 12- Cochin Institute, UMR INSERM U1016, CNRS 8104, University of Paris Descartes, CYBIO

28 Platform, Paris, France.

29 13- Department of Nutritional Sciences and Toxicology, University of California, Berkeley, USA

30 14- INSERM, Paris, France

31

32 * Correspondence and requests for materials should be addressed to MVC

33 email: mireille.vasseur@inserm.fr

34 https://orcid.org/0000-0001-6963-4114

35

36 #These authors contributed equally

37

ABSTRACT

Kings and queens of eusocial termites can live for decades, while queens sustain a nearly maximal fertility. To investigate the molecular mechanisms underlying their long lifespan, we carried out transcriptomics, lipidomics and metabolomics in *Macrotermes natalensis* on sterile short-lived workers, long-lived kings and five stages spanning twenty years of adult queen maturation. Reproductives share gene expression differences from workers in agreement with a reduction of several aging-related processes, involving upregulation of DNA damage repair and mitochondrial functions. Anti-oxidant gene expression is downregulated, while peroxidability of membranes in queens decreases. Against expectations, we observed an upregulated gene expression in fat bodies of reproductives of several components of the IIS pathway, including an insulin-like peptide, *Ilp9*. This pattern does not lead to deleterious fat storage in physogastric queens, while simple sugars dominate in their hemolymph and large amounts of resources are allocated towards oogenesis. Our findings support the notion that all processes causing aging need to be addressed simultaneously in order to prevent it.

INTRODUCTION

Aging affects almost all living organisms. It is characterized by the decay of several cellular and physiological functions, such as a deleterious accumulation of lipids[1,2], DNA damage[3], or a reduction in mitochondrial functioning which exacerbates oxidative stress[3,4]. In most multicellular organisms, surgical or genetic interventions which reduce fecundity increase lifespan[5], suggesting that fecundity and longevity are negatively correlated[6,7]. This pattern is usually explained by a trade-off, where resources allocated to fecundity are no longer available for somatic maintenance and thus longevity[6,8,9]. The regulatory mechanisms and signaling pathways controlling the allocation of resources in this trade-off remain insufficiently understood[10]. The main molecular theories of aging propose different purposes for the allocation of resources to somatic maintenance, such as controlling

63 damage accumulation, preserving mitochondrial functioning or avoiding the deleterious
64 accumulation of resources caused by inappropriate (e.g. insulin) signaling[3].
65 Our understanding of the causes of aging stems to a large extent from studies on short-lived model
66 organisms[11,12]. Eusocial insects such as termites, ants and some bees and wasps seem to defy the
67 trade-off between reproduction and longevity[13–16]. In the fungus-growing[17] termite *Macrotermes*
68 *natalensis* (Termitidae, Blattodea), individuals differentiate by irreversible developmental plasticity
69 into six distinct castes (major male and minor female workers, major and minor female soldiers,
70 queens and kings[17,18]). Queens and kings (reproductives) are for more than twenty years[13,15] confined
71 to a royal cell where they mate regularly[19] and exhibit an extraordinarily long lifespan, while the
72 median lifespan among sterile workers is 56 days[20,21]. Long-lived physogastric queens (i.e., with a
73 hyperthropic abdomen) lay thousands of fertile eggs per day[22] and achieve close to their maximum
74 possible fertility for a prolonged time without apparent signs of aging and thus with a negligible cost
75 of reproduction[23]. Recently, transcriptomic studies in different taxa of social insects have proposed
76 that downstream components of the Insulin/insulin-like growth factor (IGF-1) signaling (IIS) and the
77 target of rapamycin (TOR) pathways seem essential for bypassing the fecundity/longevity trade-
78 off[16,24–27]. This could be of broad relevance, since the dysregulation of these nutrient-sensing IIS or
79 TOR pathways leads to the impairment of lipid metabolism and the development of metabolic, age-
80 related pathologies, such as type 2 diabetes and insulin resistance, in a wide range of organisms from
81 *Drosophila* to humans[28,29]. Metabolomic and lipidomic studies in social insects are now required to
82 couple the detected gene expression plasticity between castes to the differential allocation of
83 resources to reproduction and to prolonging healthy lifespan. In termite queens which remain fertile
84 for many years, most major aging processes seem arrested[23]. In long-lived termite kings, one expects
85 the same, but the trade-off might need less bypassing if the reproductive investment is systematically
86 lower than in queens.

We investigated the molecular and physiological mechanisms allowing mature *M. natalensis* reproductives to maximize longevity, simultaneously with a large and long-term reproductive effort. To address this question, we performed tripartite -omics analyses (transcriptomics, lipidomics and metabolomics) on queens, kings and adult workers of these highly eusocial termites. We carried out metabolomic analyses on hemolymph, and concentrated the transcriptomic and lipidomic analyses on the abdominal fat body. In insects, the fat body is central for intermediary metabolism and energy balance[2,30,31]. Moreover, it has been shown in *Drosophila* that a reduction of IIS or TOR pathway activity in this tissue can extend lifespan substantially while reducing female fecundity[32–34]. We compared gene expression between reproductives and workers of twenty-year-old natural colonies. To understand their enormous developmental plasticity, we complemented this with analysis on three stages of queen reproductive maturation in laboratory colonies. By corroborating and comparing these transcriptomic findings with our metabolic and lipidomic results, we were able to gain valuable insights into age- and caste-specific differences in the fat body metabolism linked to fertility and longevity.

We expected gene expression to differ between reproductives and sterile castes in downstream components and targets of the IIS and TOR pathways, for which caste bias has been detected across other social insect taxa[16], as well as patterns specific to our model system. Additionally, we expected expression patterns in reproductives indicative of lifespan-prolonging mechanisms, of bypassing the reproduction/lifespan trade-off in queens in particular, and confirmation of these processes in the metabolomic and lipidomic analyses. We observed an upregulation of genes for different lifespan-prolonging mechanisms in mature queens and kings, supporting a robust mitochondrial functioning and increasing genome stability. An anticipated downregulation of the TORC1 signaling occurs in long-lived reproductives, but in contrast to previous studies, we observe an unexpected 800-fold upregulation of an insulin-like peptide gene which we called *Ilp9*. We correlate this phenomenon to a non-canonical downregulation of *midway* (*mdy*) involved in triglyceride lipid synthesis. The

upregulation of the *Ilp9* gene coincides with high glucose and surprisingly low trehalose levels in the hemolymph of mature queens. The apparent insulin increase is associated with an upregulation of specific gene programs involved in the synthesis of proteins and specific lipids with low oxidation potential, destined for oogenesis rather than fat storage, thus involved in bypassing the fecundity/longevity trade-off. Consistent with this, lipidomic analyses demonstrate low concentrations of preferentially stored lipids (triglycerides) in the fat bodies of mature queens and increased concentrations of lipids destined for oogenesis (diglycerides).

RESULTS

Specific regions of the gene co-expression network are activated in the fat bodies of different castes and during queen maturation

To investigate caste-specific differences between reproductives and workers in natural conditions, *M. natalensis* queens (QT4) and kings (KT4), which were over 20 years old, and short-lived female (minor[35]) workers (FW) were sampled in field colonies (Methods and Supplementary Table 1). To study the dramatic adult developmental plasticity shown by *M. natalensis* termite queens in their reproductive system and fat body during maturation, we carried out a longitudinal study in laboratory colonies established from imagoes collected from the same field colonies (QT0, virgin queens) (Methods and Fig. 1). Incipient colonies were each founded from one male and one female imago and raised for 31 months following a protocol based on the natural life history of *Macrotermes* species[20,36] (Methods and Fig. 1). Queens of laboratory colonies were sampled at 3 months after establishment (QT1), 9 months (QT2) and 31 months of age (QT3). To investigate differential gene expression between our samples, we analysed a total of 25 transcriptomes of abdominal fat bodies. RNA-sequencing data showed that variation in expression between castes and queen stages was greater than between colonies (Principal Component Analysis, PCA of top 500 genes in terms of

136 variance, Supplementary Fig. 1a). Removing FW expression from the PCA allowed a clearer
137 separation of the reproductive individuals along the first two axes (Supplementary Fig. 1b).

138 We then carried out a signed, weighted gene co-expression network analysis[37]. The resulting gene
139 co-expression network (GCN) allowed us to identify nine modules of particularly strongly co-
140 expressed genes associated with castes or with queen ages (Fig. 2, Supplementary Fig. 2,
141 Supplementary Table 2). In accordance with the PCA (Supplementary Fig. 1a), we found modules
142 strongly and uniquely correlated with FW (blue module, 1103 genes; Supplementary Fig. 2 and
143 Supplementary Table 2) and KT4 castes (plum1 module, 116 genes; Supplementary Fig. 2 and
144 Supplementary Table 2). The yellow module, enriched for GO-term functions related to localization
145 and carboxylic acid synthesis, was upregulated in physogastric queens, QT3 and QT4 (yellow
146 module, 537 genes; Supplementary Fig. 2 and Supplementary Table 2). The lightcyan module (3455
147 genes; Supplementary Fig. 2 and Supplementary Table 2) was the largest among the modules and
148 enriched for functions related to transcription and general protein synthesis. It may contain the co-
149 expressed genes affecting long-lived reproductives of both sexes QT4 and KT4, though the latter only
150 as a trend (KT4 0.39 *p*-value = 0.05; Fig. 2, Supplementary Fig. 2).

151 **Long-lived reproductives share expression patterns indicative of changed IIS signaling and**
152 **prevention of several aging processes**

153 A comparison of transcriptomic profiles between fat bodies of long-lived reproductives (KT4
154 and QT4) and short-lived FW allowed us to look at genes potentially underlying their long lifespan
155 in natural conditions, irrespective of reproductive efforts distinguishing kings from queens
156 (Supplementary Fig. 3). A total of 1454 genes were upregulated in fat bodies of KT4 and QT4 in
157 comparison to FW, including 350 genes that differed between KT4 and QT4. In addition, 2208 genes
158 were downregulated in KT4 and QT4 relative to FW, 468 of which were significantly different
159 between KT4 and QT4. By analyzing these differentially expressed genes (DEGs) we found evidence

indicating that reproductives avoid several aging processes. For instance, the expression of many genes important for genome stability, including genes involved in DNA damage response and telomere maintenance, was upregulated in KT4 and QT4 (Fig. 3 and Supplementary Tables 3-4). In addition, several genes coding for the oxidative phosphorylation system (OXPHOS) and the mitochondrial ribosomal proteins, mitochondrial transport and mitochondrial fission were upregulated in QT4 and KT4 (Fig. 3 and Supplementary Tables 3-4). This suggests that mitochondrial function was maintained in the fat bodies of long-lived reproductives with likely beneficial effects on cell integrity and oxidative status. In agreement with this, we observed a downregulation of the expression of several antioxidant genes in QT4 and KT4 relative to FW (Fig. 3 and Supplementary Table 3-4). These results were accompanied by the upregulation of gene expression involved in several processes related to protein and macromolecule synthesis (Supplementary Fig. 3).

We observed significantly upregulated expression of upstream components of IIS signaling in the fat bodies of KT4 and QT4 relative to FW. This included an 800-fold increase in gene expression of an insulin-like peptide which we called *Ilp9* (Figs. 3-4), the catalytic subunit phosphatidylinositol 3-kinase *pi3k59F*, as well as two insulin targets, *eIF6* and the transcription factor *crc*[38] (Fig. 3 and Supplementary Tables 3-4). In contrast, the expression of several actors involved in the TORC1 signaling pathway (*tor*, *raptor* and its substrate, *S6K*) were downregulated in QT4 and KT4 relative to FW, as well as the *mdy* lipid metabolism gene (Fig. 3 and Supplementary Tables 3-4). *Mdy* encodes a diacylglycerol acetyltransferase which catalyses the final step of triglyceride (TG) synthesis from diglycerides (DG)[39], and its downregulation suggests a decrease of fat storage in reproductives, to be confirmed by lipidomics below.

Expression specific to highly fecund queens suggests further adaptations in IIS signaling and a metabolism geared towards oogenesis

To better understand how highly fecund queens from mature colonies defy the reproduction/lifespan trade-off, we focused on gene expression patterns specific to QT4. For this we concentrated on genes, for which gene expression significantly differed in QT4 from both FW and KT4, thus allowing insights into the allocation of resources towards oogenesis. Again, we found that several genes involved in the IIS pathway were differentially regulated in QT4 relative to FW and KT4. For instance, the two effectors of the IIS pathway discussed in the previous section, *pi3k59F* and *crc*, were not only upregulated in both reproductives, but more strongly so in QT4 than in KT4 (Supplementary Table 4), suggesting an additional relevance of their expression for female fertility. In fact, two further *pi3k*-genes showed QT4-specific expression. While the regulatory *pi3k21B* subunit was upregulated in the fat body of QT4 compared to FW, the catalytic *pi3k92E* was downregulated in QT4 relative to FW (Supplementary Table 4). The insulin receptor *InR3* and the kinase *pdk1* were upregulated in QT4 relative to FW, but downregulated in KT4 (Supplementary Table 5).

We also found major gene expression differences in carbohydrate and lipid metabolism pathways, which are known to be activated by the IIS pathway[2]. Several genes, involved in the glycogenesis and trehalose energetic storage pathways, were upregulated in FW (Supplementary Tables 3-5). Trehalose-6-phosphate synthase was downregulated in QT4 relative to FW and KT4 (Supplementary Table 5). In QT4 queens, on the other hand, several genes which are key players in carbohydrate catabolism were upregulated relative to KT4 and FW, particularly genes encoding enzymes involved in glycolysis (e.g. *cg6650* also known as *adpgk*, *pfk* and *pkm;* Supplementary Table 5), as well as the hexosamine biosynthetic pathway (HBP) and pentose phosphate pathway (PPP) (Supplementary Tables 4-5). Queens also showed upregulation relative to FW and KT4 of genes promoting fatty acid (FA) synthesis from carbohydrates (*acc* and *fasn1*; Supplementary Table 5) and FA activation, esterification and elongation (Supplementary Table 5). Heightened DG transport in QT4 is suggested by an upregulation relative to FW and KT4 of expression of lipoprotein genes

209 essential for oogenesis, such as the female-specific vitellogenin (*vg*) and the diacylglycerol-carrying
210 lipoprotein (*hdlbp*) (Supplementary Tables 4-5).

211

212 **Transcriptomic analysis of queen maturation stages suggests different timings of activation of**
213 **oogenesis and lifespan preserving mechanisms**

214 Concomitantly with the growth of colonies and coinciding with their development of
215 physogastry, the imaginal fat body of virgin queens (QT0) with its canonical fat storage function
216 becomes replaced by a royal fat body (QT4), which is highly oriented towards specific protein
217 synthesis and secretion[40]. A comparative analysis of different termite species recently suggested that
218 endopolyploidy (or nuclear genome replication without cell division) permits the rate of vitellogenin
219 synthesis to increase[41]. Developmental changes in oogenesis might rely on endopolyploidy and we
220 therefore determine the percentages of the nuclei count at each ploidy level (2C, 4C, and 8C) in the
221 fat bodies of adult queens in five stages. To investigate when molecular mechanisms affecting
222 lifespan and oogenesis are activated, we compared gene expression between adult queens in these
223 five stages (Fig. 1). Different regions of the gene co-expression network were upregulated in each
224 stage (Supplementary Fig. 4). Next, we focused on comparing expression differences between
225 adjacent stages.

226 First, levels of expression of *Ilp9*, *InR3* and *vg* genes were not different between the
227 physogastric queen stages QT3 and QT4 (Supplementary Table 6 and Fig. 5). However, *crc* gene
228 expression (Supplementary Table 6) and genes involved in glycolysis and OXPHOS, mitochondrial
229 membrane transport proteins and mitochondrial ribosomes were all strongly upregulated in QT4
230 relative to QT3 (Supplementary Table 6). We can conclude from this that among mature physogastric
231 queen stages, substantial upregulation of important lifespan preserving processes occurs with age but

not of processes linked to oogenesis. In particular, mitochondrial functions seem to be upregulated substantially with age.

Due to a lack of workers which feed all colony members[40], queens initially live several weeks after mating without food. In the imaginal fat body of virgin queens (QT0), GO analysis revealed that several signal transduction pathways involved in fat body cell transformation and apoptosis were upregulated relative to queens at the end of this starvation period (stage QT1; Supplementary Fig. 4 and Supplementary Table 6). Furthermore, within the IIS pathway, expression of *InR2*, *InR3*, *pi3k21B*, and *Akt1* were downregulated in QT1 relative to QT0 (Supplementary Table 6). At QT1, we observed an enrichment of GO terms related to an increase of catabolic processes such as proteolysis and autophagy and an upregulation of genes involved in pathways linked to an increased use of fatty acid reserves by β-oxidation (Fig. 5, Supplementary Fig. 4, Supplementary Table 6). We observed further responses which can be explained as stress responses to starvation and which involve mechanisms known to affect aging. AMP-activated Protein Kinase α (*Ampk*α), which is known to be activated under conditions of low energy and initiates both the degradation of damaged mitochondria and mitochondrial biogenesis[42], was significantly upregulated in QT1. We observed an upregulation of two genes (*drp1*and *fis1*) known to facilitate mitochondrial degradation by autophagy and two genes involved in mitophagy (*cg5059* and *pink1*), a specific degradation of mitochondria via autophagy (Supplementary Table 6). Moreover, we observed an upregulation of the expression of genes involved in the OXPHOS system, mitochondrial ribosome subunits and mitochondrial transport proteins, suggesting an increase in mitochondria biogenesis (Supplementary Table 6). Finally, we observed an increased expression of antioxidant genes (Supplementary Table 6) which are known to be upregulated by AMPK pathway in situations of oxidative stress[43].

Given the increase in the number of workers per colony and of fungus development (Methods, Supplementary Fig. 5b and c), we believe that QT2 are fed by workers. At QT2, antioxidant defense processes, as well as *Ampk*α gene expression were downregulated (Supplementary Table 6). At this

257 stage, GO terms showed that several upregulated processes were linked to protein metabolism
258 (Supplementary Fig. 4). *Ilp9*, *pi3k21B* gene expression, and *de novo* lipogenic genes were upregulated
259 in QT2 compared to QT1, suggesting a first activation of the IIS pathway components in the fat body
260 of QT2 (Supplementary Table 6 and Fig. 5). At the same time, we observed a downregulation of *mdy*
261 gene expression, even relative to the physogastric queen stages (Fig. 5). In addition, several genes
262 involved in the cell cycle, including *mcm2, 5, 6, 7* and *10*, several cyclins and cyclin-dependent
263 kinases, such as *cycE*/*cdk2* and *orc1*, and the proto-oncogene *myc* were upregulated (Supplementary
264 Table 6). Simultaneously with the increase of *vg* expression in QT2 fat bodies, we observed an
265 increase of polyploidy levels. The proportion of 4C nuclei now exceeded 70 % (Supplementary Fig.
266 6) in comparison to 35% in QT0 and QT1. Taken together, these data suggest that QT2 is a transitory
267 stage where the final phase of fat body maturation is prepared or initiated in many processes. Our
268 PCA results support these effects (Supplementary Fig. 1b).

269 In QT3, the abdomen has become enlarged. We found that over 90% of all cells in the fat
270 bodies of QT3 and QT4 have 4C nuclei (Supplementary Fig. 6). During this period, expression of
271 *Ilp9* and *InR3* genes was upregulated in comparison to QT2 whereas *InR2* gene expression decreased
272 (Supplementary Table 6). Genes involved in glycolysis, HBP and PPP (Supplementary Table 6) were
273 upregulated. Similarly, the expression of genes involved in *de novo* lipogenesis, as well as FA
274 activation, elongation, esterification and transport were upregulated (Fig. 5). These expression
275 patterns did not change further in QT4.

276 Overall, our data suggest that the QT2 stage acts as a transitional period where *Ilp9* and
277 specific downstream IIS pathway components become upregulated. This is associated with a strong
278 downregulation of the *mdy* gene involved in triglyceride storage. The expression patterns
279 corresponding to increased oogenesis are observed when physogastry is present. Several important
280 lifespan affecting processes seem to be upregulated in QT4, long after maturation.

281

Major changes in metabolites and lipid composition highlight a lack of triglycerides and an abundance of glucose in long-lived queens

We performed metabolomic analysis on hemolymph samples of workers and queens in different stages (FW and QT0-QT4, sampling in Supplementary Table 1) to confirm and extend the results on expression patterns of genes involved in carbohydrate and lipid metabolism. Metabolomes differed between FW and QT4, and between each pair of successive queen maturation stages (pairwise perMANOVA, each p-value < 0.05; Fig. 6). FW and QT0 seemed little different overall, while starved QT1 were well separated from the QT2 individuals in transition towards massive reproduction. Physogastric QT3 were globally intermediate between QT0, QT2 and QT4 (Fig. 6). We compared individual metabolite concentrations between FW and QT4 and between successive queen maturation stages (Supplementary Fig. 7, Supplementary Table 7). We highlight the importance of simple sugars. Glucose and galactose are the metabolites present in the largest concentrations in QT4. This high concentration of glucose[44] occurred similarly in FW but not in any of the younger queen stages. Confirming our gene expression findings, the concentration of trehalose was lower in QT4 than in FW, but surprisingly also lower in QT4 than in any other queen stage (Supplementary Fig. 7, Supplementary Table 7). Alanine, glycerol, aspartic acid, phenylalanine and glutamic acid occured in larger concentrations in QT4 than FW (Supplementary Fig. 7, Supplementary Table 7), corresponding with ongoing increased protein turnover and lipid synthesis. Relative to QT0, starved queens (QT1) had increased levels of leucine, threonine, isoleucine and citric acid, which decreased again in QT2 (Supplementary Fig. 7, Supplementary Table 7). This is indicative of proteolysis during starvation.

We performed a lipidomic analysis in hemolymph of FW and QT4 and in fat bodies of QT0, QT2 and QT4 (Supplementary Table 1). The lipidomic analysis on hemolymph revealed eighty-one esterified lipid species of which 34 differed in quantity and composition between FW and QT4 (Fig. 7, Supplementary Table 8). Strikingly, DG were significantly elevated in QT4 relative to FW while

several TG were significantly diminished (Fig. 7, Supplementary Table 8). This decrease of TG concentrations in QT4 hemolymph as well as the upregulation of genes involved in the IIS pathway and *de novo* lipogenesis in fat bodies, plus the decrease of *mdy* gene expression observed in reproductives relative to FW, suggest a decrease in fat body TG storage in QT4. Thirteen TG concentrations were in fact significantly lower in QT4 fat bodies relative to QT0 (Fig. 8a, Supplementary Table 9).

In addition, we determined fatty acid composition in fat bodies of queens to assess the levels of oxidative cell damage. We investigated changes in proportions of polyunsaturated fatty acids (PUFA), monounsaturated fatty acids (MUFA) and saturated fatty acids (SFA) in fat bodies of QT0, QT2 and QT4. PUFA/MUFA/SFA proportions in fat bodies of QT2 and QT4 were significantly different from QT0 (PERMANOVA, p-value < 0.05; Fig. 8b). This difference seemed to be related to a larger proportion of PUFA (highly oxidizable) in QT0 compared to QT2 and QT4 (Fig. 8b). We calculated the relative peroxidability of membranes (peroxidation index, PI), which decreased drastically from 29.5 at QT0, 7.9 at QT2 to 1.9 at QT4 (Fig. 8c). This can explain the scope for downregulation of antioxidant genes in QT4.

DISCUSSION

Our results reveal several mechanisms by which long-lived termite reproductives defy aging. They support the joint occurrence of the avoidance of DNA damage accumulation, the maintenance of mitochondrial functioning and turnover, accompanied by a reduction of antioxidant defenses. Termite queens sustain high fertility throughout their long life without apparent costs of their long-term massive reproductive output. We observed a remodeling of signaling pathways across queen maturation stages which could help to prevent hyperfunction[45] despite sustained insulin signaling. The composition of lipids in long-lived queens is less sensitive to oxidative damage and the observed scarcity of stored fat (TGs) observed relative to DGs seems to optimize both sustained fecundity and

health span. All this seems possible while termite queens are fed mostly on simple sugars by female workers.

Long lifespan on a carbohydrate diet

Overall, all results confirm that long-lived queens receive a highly energetic food enriched in simple sugars. In many organisms from *Drosophila* to humans, a prolonged carbohydrate-rich diet is associated with chronic metabolic diseases reducing lifespan[29,46]. Increased insulin secretion caused by such a diet leads to the accumulation of TG, and disrupted IIS signaling over time leads to the development of insulin resistance[2,46–48]. The intermediary metabolism in QT4 queens is centered on a high use of carbohydrates with an increase of glycolysis, *de novo* lipogenesis and the OXPHOS system for energy generation and the synthesis of specific lipids and proteins. Poulsen *et al.*[49] have additionally shown that the diversity of decomposition enzymes encoded by the queen's microbiota is low and geared towards hydrolyzing simple sugars. The unexpected low trehalose concentrations in long-lived queens, coupled with their high glucose levels also occurring in female workers suggest that glucose is an important component of what female workers feed to physogastric queens in colonies with a well-developed fungus, without much trehalose synthesis or prompt trehalose hydrolysis. In mammals and even in *C. elegans*, trehalose counteracts disruptions of protein homeostasis by oxidative stress, temperature variation and dessication[50–52] and thus leads to increasing lifespan. The absence of trehalose in long-lived queens is possibly facilitated by the protected lifestyle of reproductives in the royal cell, or by compensatory mechanisms such as the maintenance of a healthy mitochondria population producing low amounts of ROS[53–56]. We found expression patterns in trehalose pathways that were specific to physogastric queens, suggesting that the patterns of hemolymph sugars in kings might be less extreme.

357 *No fat storage in long-lived queens*

358 Remarkably, we observed a transcriptional downregulation of genes coding for different
359 mechanisms of energy storage (triglycerides, glycogen and trehalose) in long-lived queens. Using
360 resources immediately to sustain fecundity is detrimental in most iteroparous life history strategies.
361 Most individuals need to maintain reserves themselves, for example, in order to buffer periods with
362 low foraging success (starvation)[30,44]. In social insects, this task can be delegated to workers assuring
363 a constant food supply.

364 Coinciding with upregulated *de novo* lipogenesis and upregulation of the *vg* gene from QT2
365 queens onwards, expression of the *mdy* gene coding a diacylglycerol acyltransferase was
366 downregulated. This can explain the decrease of TG concentrations we observed in long-lived queens
367 and suggests very limited storage of TG in physogastric queens in favor of immediate utilization.
368 Also, we observed a trend for DG to increase, which are known to be preferably used for lipid
369 transport[57] (not free fatty acid as in vertebrates). Han & Bordereau[40] observed almost forty years ago
370 low levels of lipid droplets in the fat body of long-lived *Macrotermes* termite queens. A decrease of
371 *mdy* gene expression was also observed in the fat body of mature kings, suggesting that a low level
372 of stored TG could be generally beneficial for long-lifespan in reproductives and is not just explaining
373 the absence of a cost of reproduction in queens. Our results make the gene network involving *mdy*
374 and fat concentrations in reproductives of both sexes targets for research linked to the accumulation
375 of excess fat.

376

377 *Surprising upregulation of IIS pathway components in reproductives*

378 A comparative analysis of termites, ants and bees suggested that downstream components of
379 the IIS/TOR signaling pathways play a consistent role in determining lifespan in eusocial insects[16].
380 We found changes in the IIS pathway in the fat bodies of reproductives. In *Drosophila*, seven out of

eight insulin-like peptides (DILPs) are mainly produced in the brain. The exception, DILP6, is produced in the fat body and its gene expression is upregulated during starvation[58,59]. In *M. natalensis*, we identified two genes from separate loci, one coding an ortholog to DILP7 (not expressed in *M. natalensis* fat bodies) and a further paralog found across holo- and hemimetabolous insects, without a clear ortholog in *Drosophila melanogaster*, which we called *Ilp9*. During queen maturation, we observed potential increases in insulin suggested by greatly upregulated expression of *Ilp9* in the transitional QT2 stage and when physogastry becomes established. It is approximately 800-fold more expressed in fat bodies of long-lived reproductives relative to female workers. The increase of *Ilp9* gene expression in long-lived reproductives was not associated with an activation of TORC1, although the expression of genes involved in protein synthesis was upregulated in their fat bodies. We observed an upregulation of *elF6* gene expression which is involved in insulin-stimulated translation, most notably by controlling adipogenic transcription factors like *crc* (also known as *ATF4*), a member of the mTOR-independent pathway[38,60]. We propose that *Ilp9* activates the eIF6-*crc* gene program in the fat bodies of mature queens and kings. This in turn increases the synthesis of proteins that are involved in lipid synthesis and essential for fecundity. This occurs despite a downregulation of TORC1, elsewhere described as the main pathway for protein synthesis[61] and also found downregulated in whole bodies of a lower termite species[24,25].

Maintenance of mitochondrial turnover with low ROS production in long-lived reproductives

Several studies demonstrated that during calorie restriction, mitochondrial stress induced by a transitory increase of ROS leads to a cellular adaptive response named mitohormesis which, in the long term, allows for more effective stress resistance and lifespan extension[62–64]. During the starvation period at the QT1 stage, the absence of nutrition was associated with an upregulation of genes coding for mitochondria biogenesis (OXPHOS system, mitochondrial ribosome subunits and transport) and mitochondrial fission (a mechanism involved in mitochondrial degradation by autophagy). This

406 allows an increase in stress resistance by increasing both the degradation of damaged mitochondria
407 and the synthesis of new ones[62]. We also observed an upregulation of the expression of genes coding
408 for antioxidant enzymes, which may suggest a mitohormetic response to an increase of ROS
409 production. Interestingly, we observed that genes coding mitochondrial synthesis and fission were
410 again upregulated in QT4 and KT4 reproductives, suggesting a maintenance of mitochondrial
411 turnover while genes coding for antioxidant enzymes were downregulated. Similar downregulation
412 was observed in honeybee and ant queens[65,66]. Our findings suggest that the mitochondria of long-
413 lived reproductives remain efficient and produce a comparatively low amount of ROS, thus
414 preventing oxidative damage and provoking at most a weak mitohormetic response.

415

416 *Lower sensitivity to oxidative damage in long-lived queens*

417 Several studies in mammals, birds and invertebrates[67,68] have demonstrated that PI values
418 correlate negatively with longevity. We highlighted significant decreases in the fraction of
419 polyunsaturated fatty acids (PUFA) in QT2 and again in QT4 queens, leading to a strong, progressive
420 decline of the peroxidation index (PI). PUFA are a thousand times more likely to oxidize than
421 MUFA[67]. Their oxidation can set off an oxidative cascade with the formation of radicals capable of
422 damaging surrounding macromolecules and tissues[67]. Therefore, the decreases in PUFA fractions can
423 lead to a reduction in oxidative damage and increase lifespan of queens while genes coding for
424 antioxidant enzymes are downregulated. We therefore predict that PI values decrease similarly in
425 kings, which could be confirmed by future studies on different maturity stages of kings.

426

427 In conclusion, our study indicates that developmental plasticity in this natural system allows it to
428 overcome several well-known hallmarks of aging[3], including mitochondrial dysfunction, genomic
429 instability and deregulated nutrient sensing. Our results highlight the importance of an insulin-like

peptide (ILP9), which is upregulated in the fat bodies of long-lived reproductives and likely changes downstream signaling, leading to the gene expression profiles and metabolism which extend lifespan. These findings have implications for aging research, supporting the notion that aging can only be arrested when all factors which increase mortality over time are addressed.

METHODS

Sampling

Macrotermes natalensis lives in large colonies in Southern Africa where it builds massive mounds[69]. Field colonies opened to collect animals had been followed for over 20 years by Jannette Mitchell in an experimental filed of the University of Pretoria (coordinates in Supplementary Table 10)[70]. Old minor adult workers (FW), virgin queens (QT0), 20-years old queens (QT4) and kings (KT4) were sampled from at least twenty-year-old colonies. Less than an hour was taken to reach the royal cells containing QT4 and KT4. We observed that habitacle volumes were comparable between colonies (data not shown), suggesting that the colonies were of the same age. QT4 and KT4 also showed limited variability in weight and length between colonies.

Establishment and maintenance of incipient termite colonies

When natural colonies are mature (five to seven years after establishment) and in appropriate environmental conditions, winged male and female imagoes leave the mound during spring and disperse in synchronous swarms[70]. Imagoes were collected in Pretoria (South Africa) in 2016 and 2018 during the spring swarming flights (coordinates in Supplementary Table 10). Mounds were covered with nets to retrieve imagoes. These were placed in large boxes preserving humidity and immediately transferred to the laboratory. In the field, males locate female imagoes[71] and paired

453 couples perform dealation and establish new colonies as queen and king[70]. Imagoes collected were
454 sexed by visual observation of their abdominal sternites. Weight and length were recorded and wings
455 were manually removed. Establishment of laboratory incipient colonies occurred for both field trips,
456 following a protocol adapted from Lepage[36] and Han & Bordereau[20] (Fig. 1 and Supplementary Fig.
457 8). We established 1600 incipient colonies. Each paired couple was introduced in a closed plastic box
458 (6 x 5 x 4.5 cm) filled with sieved soil collected near the mounds. The incipient colonies were kept
459 in a breeding room with controlled conditions: 28°C, 85% relative humidity and 12:12 photoperiod.
460 Water was used to keep the soil slightly moistened. Development of the colonies was visually
461 monitored. In the field, workers explore the environment a few months after colony establishment to
462 collect spores and to inoculate the fungus comb they build in the nest[72]. Workers feed all colony
463 members through trophallaxis (transfer of food from mouth to mouth), after a complex digestion of
464 lignocellulose by the fungus and intestinal microbiota[49]. At three months in the laboratory colonies,
465 when workers started to explore, small pieces of dry wild oats were supplied on the surface of the soil
466 and wood was additionally supplied after 4.5 months. A *Termitomyces* sp. fungus comb with nodules
467 was collected from one mature field colony and a small part of this comb was introduced in each box.
468 After 3.5 months, mortality was 56% for the 2016 incipient colonies (± 15% across field colonies of
469 origin) and 30 ± 7% for the 2018 incipient colonies. When the termite populations outgrew their
470 boxes, they were opened on one side and placed inside bigger ones (18 x 12 x 7.5 cm after three
471 months, 36 x 24 x 14 cm after 14 months, and 1000 x 70 x 40 cm after 21 months) filled with sieved
472 moistened soil. Colonies were checked every two days to supply water and food if needed and to
473 remove moldy food. Queens were sampled after 3 months (QT1), 9 months (QT2) and after 31 months
474 (QT3). During the first years of a colony's life, larvae emerge which become sterile workers or
475 soldiers[35]. At QT1, the number of minor and major workers, soldiers, presoldiers, and larvae were
476 counted in colonies where queens were sampled. At QT2, these were also counted and the fungus
477 was weighed.

478 **Species identity**

479 Total DNA was isolated from the head and the legs of one imago of each of the 9 colonies. PCR was
480 performed using the cytochrome oxidase I gene primers: LCO 5'- GGT CAA CAA ATC ATA AAG
481 ATA TTG G -3' and HCO 5'- TAA ACT TCA GGG TGA CCA AAA AAT CA -3'[73] and the 650-
482 bp amplified fragment was sequenced and analyzed using the Barcode of Life Database identification
483 system (www.barcodinglife.org). Species identity of each colony was confirmed to be *M.*
484 *natalensis*[49].

485

486 **Hemolymph and fat body collection**

487 Fat bodies were collected from cold-anesthetized individuals (FW, QT0, QT1, QT2, QT3, QT4 and
488 KT4). Hemolymph was collected on FW, QT0, QT1, QT2, QT3 and QT4 (Supplementary Table 1)
489 under a binocular microscope with tapered glass Pasteur pipettes inserted in the membranous part just
490 behind the head. The mean volume of hemolymph collected per individual was 0.5 µL for FW, 1.5
491 µL for QT0, QT1, QT2, 50 µL for QT3, and 1 mL for QT4. Hemolymph samples were collected in
492 cryotubes, quickly frozen in liquid nitrogen and kept at -80°C until use. Subsequently, termites were
493 killed by decapitation and their abdominal fat bodies were collected. For RNA and DNA extraction,
494 the fat body was stored in a tube containing RNAlater buffer (Invitrogen) and kept at -80°C until use.
495 For lipid and metabolite analyses, nitrogen-frozen fat bodies were crushed in a tube which was
496 immediately frozen in liquid nitrogen and kept at -80°C until use. For ploidy analyses, the fat body
497 was collected from one individual, stored in a tube containing 200 µL of Cycletest PLUS DNA
498 Reagent Kit buffer (Becton Dickinson) and kept at -80°C until use.

499

500

RNA profiling

In the 2016 and 2018 cohort, total RNA was isolated from fat bodies of FW, QT0, QT1, QT2, QT3, QT4 and KT4 using miRNeasy Micro kit (Qiagen) and RNAse-free DNAse according to the manufacturer's instructions (Qiagen). Number of replicates per group are provided in Supplementary Table 1. RNA-Seq library preparations were carried out from 500 ng total RNA using the TruSeq Stranded mRNA kit (Illumina, San Diego, CA, USA) which allows mRNA strand orientation (sequence reads occur in the same orientation as anti-sense RNA). Briefly, poly(A)$^+$ RNA was selected with oligo(dT) beads, chemically fragmented and converted into single-stranded cDNA using random hexamer priming. Then, the second strand was generated to create double-stranded cDNA. cDNA were 3'-adenylated and Illumina adapters added. Ligation products were PCR-amplified. All libraries were subjected to size profile analysis conducted by Agilent 2100 Bioanalyzer (Agilent Technologies, Santa Clara, CA, USA) and qPCR quantification (MxPro, Agilent Technologies, Santa Clara, CA, USA) using the KAPA Library Quantification Kit for Illumina Libraries (KapaBiosystems, Wilmington, MA, USA), then sequenced using 150 bp paired end reads chemistry on a HiSeq 4000 Illumina sequencer (Illumina, San Diego, CA, USA). An Illumina filter was applied to remove the least reliable data from the analysis. The raw data were filtered to remove any clusters with too much intensity corresponding to bases other than the called base. Adapters and primers were removed on the whole read and low-quality nucleotides were trimmed from both ends (when quality value was lower than 20). Sequences between the second unknown nucleotide (N) and the end of the read were also removed.

RNA-seq analyses

The *M. natalensis* genome[49] was downloaded from the gigadb database (http://gigadb.org/dataset/100057; accessed March 2019). RNAseq reads were mapped against the genome using *hisat2* (version 2.1.0[74]) at default settings. Gene expression levels were then generated

525 by counting reads mapping to each gene of the *M. natalensis* genome (annotation version 2.3) using
526 *htseq-count*[75]. Differential expression analyses were carried out in R (3.5.1) with the DESeq2
527 package[76], comparing between all pairs of castes and queen stages, as well as comparing each caste
528 and queen stage against all others. Genes were considered significantly differentially expressed if the
529 adjusted *p*-value was less than 0.05. Principal component analyses (PCA) were also carried out within
530 the DESeq2 package[76]. Counts were transformed using the *varianceStabilizingTransformation*
531 function, and the PCA was calculated and plotted using the *plotPCA* function. This function carries
532 out a PCA on the top 500 genes, based on variance. A weighted gene co-expression network (WGCN)
533 was generated with these gene expression counts, using the R package WGCNA[37]. Normalized counts
534 were extracted from the DESeq2 data set with the *counts* function. These data were filtered for genes
535 with zero variance or with missing values with the WGCNA function *goodSamplesGenes*. With the
536 remaining 9631 genes, a signed WGCN was created using a soft power of 14, implementing the
537 biweight midcorrelation calculation and setting the minimum module size to 30. Modules with a
538 dissimilarity less than 0.5 were merged using the *mergeCloseModules* function. We related the
539 expression profiles of the resulting nine modules to castes and queen stages by correlating (Pearson's
540 *r*) the module eigengenes (first principal component of the expression matrix of each module) with a
541 binary vector, containing 0s and 1s depending on the membership of each sample (FW, QT0, QT1,
542 QT2, QT3, QT4 or KT4). A significant positive correlation signifies an overall upregulation while a
543 negative correlation signifies a downregulation of expression within the module for a given caste or
544 queen stage.

545 To visualize the WGCN, we first reduced the WGCN to include only the most highly connected
546 nodes. We did this by retaining genes with a topological overlap of at least 0.2 with at least another
547 gene, and by including the top 15 most connected genes within each module. This reduced WGCN
548 (5823 genes) was exported to Cytoscape (version 3.8.0[77]) with the *exportNetworkToCytoscape*
549 function in WGCNA (threshold 0.15). In Cytoscape, the network was rendered using the Edge-

weighted Spring Embedded Layout and nodes were colored by module membership or expression fold change. GO term enrichment analyses were carried out with topGO (version 2.34.0[78]), using the classic algorithm. Node size was set to 5, Fisher exact tests were applied, and we only kept GO terms that matched with 2 genes at least and with a *p*-value < 0.05. We established orthology of *M. natalensis* genes to *D. melanogaster* (v. 6.12) and *H. sapiens* (hg38) using the method of reciprocal best BLAST hit[79]. For this, the proteomes were blasted against each other using BLASTp (BLAST 2.7.1+[80]) and an e-value threshold of 1e–5. Reciprocal best BLAST hits were extracted from the output files using a custom python script.

Analysis of ILPs

Two ILP genes (Mnat_00258 and Mnat_03820) were found in the *M. natalensis* proteome based on sequence similarity to ILPs in *D. melanogaster*, using BLASTp (BLAST 2.7.1+[80]) with a e-value threshold of 1e-5. We checked for further ILP genes within the genome by mapping the protein sequences of these two *M. natalensis* genes and eight known *D. melanogaster* ILPs (downloaded from NCBI; accessed February 2021) against the *M. natalensis* genome. This was carried out with EXONERATE (v 2.2.0 [81]) using the protein2genome model at default settings. No further ILP copies were found but the annotations of the two *M. natalensis* genes were improved based on these exonerate alignments (new annotations and protein sequences are available at github.com/MCH74/Mnat_analyses). We searched for ILP orthologs within 25 further insect proteomes (see table in Fig.4 for full details) using BLASTp and an e-value threshold of 1e-5. The protein sequences were aligned with t-coffee[82] in accurate mode, which incorporates both sequence profile and structural information. We trimmed the alignment with trimAL in the *automated1* mode[83], then created a gene tree with iqtree2[84]. This program automatically selects the best-fit model with ModelFinder and carries out bootstraps. With these methods we recreated a gene tree Q.pfam+R4 model and 10,000 bootstraps. The tree was visualized with the online tool, iTOL v6[85].

Metabolomic analysis

A volume of 20 µL of hemolymph of FW, QT0, QT1, QT2, QT3 and QT4 was used to determine metabolic profiles obtained by gas chromatography coupled with mass spectrometry (GC-MS). Number of replicates per group are provided in Supplementary Table 1. We used the experimental procedure described in Khodayari *et al.*[86], and adapted in Genitoni *et al.*[87]. Samples were homogenized in 450 µL of ice-cold methanol/chloroform (2:1, v/v) before the addition of 300 µL of ultra-pure water. After they have been vigorously vortexed, the samples were centrifuged for 10 min at 4,000 g (4°C). Then, 100 µL of the upper phase, which contains metabolites, was transferred to new glass vials (Thermofisher), speedvac dried at RT, and vials sealed with PTFE caps. The derivatization of the samples was conducted with a CTC CombiPAL autosampler (CTC Analytics AG, Zwingen, Switzerland), as described in Khodayari *et al.*[86]. The GC-MS platform consisted of an Agilent 7890B gas chromatograph coupled to a 5977B mass spectrometer. The injector was held at 250°C, and the temperature of the oven ranged from 70 to 170°C at 5°C/min, from 170 to 280°C at 7°C/min, and from 280 to 320°C at 15°C/min; at the end of the temperature ramps, the oven remained at 320°C for 4 min. A 30 m fused silica column (HP5 MS 30 m, I.D. 0.25 mm, thickness 0.25 µm, 5% Diphenyl / 95% dimethylpolysiloxane, Agilent Technologies) was used with helium as the gas carrier at 1 mL per min. The temperatures of the transfer line and ion source were 280 and 230°C, respectively. The split mode (split ratio: 2:1) was used for the injection of 1 µL of each sample, and detection was realized by electronic impact (electron energy: 70 eV) in full scan mode. The peaks list was annotated based on their MS fragmentation patterns with MassHunter. Detected metabolites were identified, and calibration curves were used to calculate the concentration of each metabolite.

Statistical analysis

Permutational MANOVA[88] was used to test for differences in multivariate metabolite concentrations between stages and castes. We subsequently tested for differences in individual metabolites between

599 pairs of subsequent stages or between FW vs. QT0 and FW vs. QT4. The concentrations of all
600 metabolites were log transformed and compared between groups by using Welch tests. Tail
601 probabilities were corrected for multiple testing using the Benjamini-Hochberg method. Tests were
602 considered significant for a p-value < 0.05 and carried out using R software (v 3.6.3).
603
604 **Lipidomic analysis**

605 Lipids were extracted for fatty acid profile analysis gas chromatography with flame ionization
606 detection (GC-FID) and gas chromatography coupled to mass spectrometry (GC-MS). Lipidomic
607 analyses were done by liquid chromatography coupled to mass spectrometry (LC-HRMS/MS). Lipids
608 were extracted from 20 µL of hemolymph (from FW and QT4) or from fat bodies (from QT0, QT2
609 and QT4) using a biphasic solvent system of cold methanol, methyl tert-butyl ether (MTBE), and
610 water, adapted from Cajka *et al.*[89]. Briefly, the samples were transferred in 750 µL of MTBE and 150
611 µL of methanol into a 2 mL screw cap tube. For lipidomic analysis, 1µL of internal standard (PC 31:
612 1|PC17:0-PC14:1) at 3,775 µg/mL was added to each sample. After homogenization with the
613 "Precellys tissue homogenizer" at 5,000 rpm for 5 minutes, 400 µL of H_2O was added to each sample.
614 The samples were then centrifuged at 13,000 rpm for 5 min. The upper phase containing the lipids
615 (MTBE) was transferred into a new tube and dried under a stream of nitrogen at 20°C. For fatty acid
616 profile analysis, extracted lipids were transferred in 100 µL of MTBE, methylated into fatty acids of
617 methyl esters (FAMEs) after the addition of 10 µL of tetramethylammonium hydroxide (TMAH).
618 After a centrifugation at 4,000 rpm during 5 min, supernatants were collected and diluted 3 times into
619 heptane prior to injection into GC-FID and GC-MS. For lipidomic analysis, lipids extracted were
620 taken up into 100 µL of isopropanol before injection into LC-HRMS/MS.
621
622

FAMEs analysis

From fat bodies of different queen stages, fatty acid profiles were separated and analyzed by a gas chromatography with flame ionization detection (GC-FID 2010 Plus Shimadzu) equipped with a BPX 70 capillary column (SGE, 30 m × 0.25 mm, 0.25 µm) as described in Merlier *et al.*[90]. The fatty acids were identified by comparison of the retention times of a standard solution of 37 fatty acid methyl esters (Sigma; 47885-U Supelco) in GC-FID and confirmed by high accuracy mass of molecular ions and their fragments after injection into a GC-MS (Q-Exactive™, Thermo)[90]. The composition of fatty acids was expressed as a relative percentage of their peak areas with respect to the total peak area of all the fatty acids. The fat body samples were normalized by dividing peak areas with total DNA concentration (ng/mL) measured with a Qubit Fluorometer (Thermofisher) and Qubit dsDNA Assay kit (Invitrogen). The membrane peroxidation index (PI) of lipid extracts in fat bodies of queens was calculated as the sum of bis-allylic methylene groups per 100 fatty acids according to the equation[67]:

PI= (percentage of dienoics x1) + (percentage of trienoics x2) + (percentage of hexaenoics x5)

Untargeted lipidomics analysis

The untargeted lipidomics analysis was conducted using a liquid chromatography-high resolution tandem mass spectrometry (LC-HRMS/MS) analysis used as described and modified from Ulmer *et al.*[91]. An HPLC 1290 (Agilent Technologies) coupled to a hybrid quadrupole time-of-flight high definition (QtoF) mass spectrometer Agilent 6538 (Agilent Technologies) equipped with an ESI dual source was used. Lipids were separated on a C18 Hypersil Gold (100 x 2.1 mm, 1.9 µm, Thermofisher) at 50°C, using an elution gradient composed of a solution of 20 mM of ammonium acetate and 0.1% formic acid (ACN: H_2O, 60:40, v/v) (solvent A) and a solution of 20 mM of ammonium acetate and 0.1% formic acid (IPA: ACN:H_20, 90:8:2, v/v) (solvent B). Separation was conducted under the following gradient: 0–2 min from 32% (B), 2–3 min from 32% to 40% (B), 3–8 min from 40% to 45% (B), 8–10 min from 45% to 50% (B), 10–16 min from 50% to 60% (B), 16–

22 min from 60% to 70% (B), 22–28 min from 70% to 80% (B), 28–30 min from 80% to 99% (B), 30–31 min from 99% to 32% (B), 31–36 min from 32% to 32% (B). The flow rate was set at 250 µL/min. Two µL of samples were injected. MS / MS spectra were acquired in positive mode and in negative mode in data dependent and MS^2 scans were performed on the sixth most intense ions. The source temperature, fragmentor and the skimmer were set up at 350°C, 150 V and 65 V, respectively. The acquisition was made in full scan mode between 100 m/z and 1700 m/z, with a scan of two spectra per second. Two internal references were used for in-run calibration of the mass spectrometer (121.0509, 922.0098 in positive ion mode and 112.9856, 1033.9881 in negative ion mode). MassHunter B.07 software allowed us to control the parameters of the machine acquired.

Data processing and annotation

MsDial v4.0 software[92] was used for data processing and annotation of lipids. The data collection was performed by fixing the MS1 and MS2 tolerance, at 0.01 Da and 0.025 Da, respectively. The peak detection was fixed at 1000 amplitude and a mass slice width at 0.1 Da. The deconvolution parameters correspond to a sigma window value at 0.5 and a MS/MS abundance cut off at 10 amplitude. Isotopic ions were kept until 0.5 Da. The peaks list was annotated based on their unique MS/MS fragmentation patterns using the in-built LipidBlast mass spectral library in MS-DIAL software. The accurate mass tolerance MS1 and MS2 were fixed -at 0.01 Da and 0.05 Da respectively. The identification score cut off was fixed at 80%. Lipids were normalized by the intensity of the internal standard (PC 31: 1|PC17:0-PC14:1).

Statistical analysis for lipidomic data

To compare the percentages of SFA, MUFA, PUFA lipid content in fat bodies of different queen stages we used a permutational MANOVA on ilr-transformed compositional data[93] followed by pairwise post-hoc perMANOVA comparisons of each stage with QT4 (Holm-Bonferroni correction for multiple comparisons). To compare log-transformed individual lipid values between FW and

671 QT4, or between QT0, QT2 and QT4, Welch tests were used, corrected for multiple testing using the
672 Benjamini-Hochberg method. To compare the peroxidation index (PI) in fat bodies of different queen
673 stages we used Kruskal-Wallis test followed by Dunn's post hoc comparisons. All tests were
674 considered significant for a p-value < 0.05 and were carried out using R software (v 4.0.2). Heatmaps
675 were made using the heatmap function in the Metaboanalyst v 4.0. with Euclidean distance and
676 clustering using Ward's method.

677

678 **Ploidy analysis**

679 Fat bodies from QT0, QT1, QT2, QT3 and QT4 were processed by Flow Cytometric Analysis with a
680 Cycletest PLUS DNA Reagent Kit (BD Biosciences, Le pont de Claix). Number of replicates per
681 group are provided in Supplementary Table 1. All procedures were adapted from Nozaki &
682 Matsuura[41]. Stained nuclei were analyzed for DNA-PI fluorescence using an Accuri C6 Flow
683 Cytometer (BD Biosciences) at an excitation wavelength of 488 nm and a detector equipped with an
684 585/45 bandpass filter. Approximately 1,000 cells were acquired for each measurement. Flow
685 cytometric analyses were performed with the Accuri C6 software v1.0.264.21 (BD Biosciences).
686 Debris were removed on an FSC-A/SSC-A dotplot and doublet were eliminated with and PI-FL2-H/
687 FL2-A dot plot. The nuclei were analyzed with a histogram PI-A. The 1C DNA peak was determined
688 by the analysis of king's testis (sperm), allowing the identification of the 2C, 4C, and 8C peaks of the
689 others samples.

690 *Statistical analysis for ploidy*

691 To compare percentages of nuclei with different multiples of haploid genomes between queen stages,
692 we used permutational MANOVA followed by pairwise post-hoc perMANOVA (Holm-Bonferroni
693 correction for multiple comparisons).

694 **Acknowledgements**

695 The authors would like to thank Dr Christian Bordereau and Dr Jannette Mitchell for helpful
696 discussions on the termite model. The authors acknowledge the Department of Public Works and
697 Infrastructure, Pretoria and the University of Pretoria for allowing access to their sites of collect of
698 *M. natalensis*. The authors also thank Cyril Fresillon and Pierre Deparscau, photographers for the
699 CNRS images. We thank Qi Li for termite colony maintenance. This study was supported by the
700 International Human Frontier Science Program RGP0060/2018 to M.V.C. S.S was also supported by
701 a fellowship from Université de Paris Est-Créteil (UPEC). A.L. acknowledges financial support from
702 France Génomique (ANR-10-INBS-09-08). We would like to thank the EcoChim platform of
703 University of Rennes for access to metabolomics facilities.

704

705 **Author contributions**

706 M.V.C designed the study. D.S-D., A.R., R.L., L-A.P., Z.W.D.B., and M.V.C. carried out termite
707 experiments, M.V.C and A.L. transcriptomic, D.R. and R.L. metabolomic and S.A. and R.L.
708 lipidomic experiments. M.A. and M.V.C. measured DNA contents. S.S., M.H., T.V.D and M.V.C.
709 analyzed the data, wrote the original draft and compiled the figures and tables presented. All authors
710 contributed with expertise, input, and edits throughout the text.

711

712 **Competing interests**

713 The authors declare that they have no conflict of interest.

714

715 **Data availability**

716 The authors declare that all data supporting the findings of this study are available within the paper
717 and supplementary information files, or are available from a dedicated github repository:

718 https://github.com/MCH74/Mnat_analyses. RNA-seq reads generated in this study are available in
719 Sequence Read Archive (BioProject ID: PRJNA685589 and BioSample
720 accessions: SAMN17088123- SAMN17088147).

721

722 **Additional information**

723 Supplementary Information accompanies this paper.

724
725 REFERENCES
726
727 1. Johnson, A. A. & Stolzing, A. The role of lipid metabolism in aging, lifespan regulation,
728 and age-related disease. *Aging Cell* **18**, e13048 (2019).
729 2. Heier, C. & Kühnlein, R. P. Triacylglycerol metabolism in *Drosophila melanogaster*.
730 *Genetics* **210**, 1163–1184 (2018).
731 3. López-Otín, C., Blasco, M. A., Partridge, L., Serrano, M. & Kroemer, G. The hallmarks
732 of aging. *Cell* **153**, 1194–1217 (2013).
733 4. Balaban, R. S., Nemoto, S. & Finkel, T. Mitochondria, oxidants, and aging. *Cell* **120**,
734 483–495 (2005).
735 5. Flatt, T. Survival costs of reproduction in *Drosophila*. *Experimental Gerontology* **46**,
736 369–375 (2011).
737 6. Kirkwood, T. B. L. Evolution of ageing. *Nature* **270**, 301–304 (1977).
738 7. Kirkwood, T. B. L. & Austad, S. N. Why do we age? *Nature* **408**, 233–238 (2000).
739 8. Maklakov, A. A. *et al.* Antagonistically pleiotropic allele increases lifespan and late-life
740 reproduction at the cost of early-life reproduction and individual fitness. *Proceedings of*
741 *the Royal Society B: Biological Sciences* **284**, 20170376 (2017).
742 9. Williams, G. C. Natural selection, the costs of reproduction, and a refinement of lack's
743 principle. *The American Naturalist* **100**, 687–690 (1966).
744 10. Edward, D. A. & Chapman, T. Mechanisms underlying reproductive trade-offs: costs of
745 reproduction. Mechanisms of Life History Evolution (Oxford University Press, 2011).
746 11. Hansen, M., Flatt, T. & Aguilaniu, H. Reproduction, fat metabolism, and life span: what
747 is the connection? *Cell Metabolism* **17**, 10–19 (2013).
748 12. Taormina, G. *et al.* Longevity: lesson from model organisms. *Genes* **10**, 518 (2019).
749 13. Keller, L. Queen lifespan and colony characteristics in ants and termites. *Insectes*
750 *sociaux.* **45**, 235–246 (1998).
751 14. Keller, L. & Genoud, M. Extraordinary lifespans in ants: a test of evolutionary theories
752 of ageing. *Nature* **389**, 958–960 (1997).
753 15. Carey, J. R. Demographic mechanisms for the evolution of long life in social insects.
754 *Experimental Gerontology* **36**, 713–722 (2001).
755 16. Korb, J. *et al.* Comparative transcriptomic analysis of the mechanisms underpinning
756 ageing and fecundity in social insects. *Philosophical Transactions of the Royal Society*
757 *B: Biological Sciences* **376**, 20190728 (2021).
758 17. De Fine Licht, H. H., Andersen, A. & Aanen, D. K. *Termitomyces* sp. associated with
759 the termite *Macrotermes natalensis* has a heterothallic mating system and multinucleate
760 cells. *Mycological Research* **109**, 314–318 (2005).

18. Korb, J. *et al.* A genomic comparison of two termites with different social complexity. *Frontiers in Genetics* **6**, 9 (2015).
19. Hartke, T. R. & Baer, B. The mating biology of termites: a comparative review. *Animal Behaviour* **82**, 927–936 (2011).
20. Han, S. H. (Universite d'Abidjan & Bordereau, C. From colony foundation to dispersal flight in a higher fungus-growing termite, *Macrotermes subhyalinus,* (Isoptera, Macrotermitinae). *Sociobiology (USA)* (1992).
21. Traniello, J. F. A. & Leuthold, R. H. Behavior and ecology of foraging in termites. in *Termites: Evolution, Sociality, Symbioses, Ecology* (eds. Abe, T., Bignell, D. E. & Higashi, M.) 141–168 (Springer Netherlands, 2000).
22. Kaib, M., Hacker, M. & Brandl, R. Egg-laying in monogynous and polygynous colonies of the termite *Macrotermes michaelseni* (Isoptera, Macrotermitidae). *Insectes sociaux* **48**, 231–237 (2001).
23. Kuhn, J. M. M., Meusemann, K. & Korb, J. Disentangling the aging gene expression network of termite queens. BMC genomics 22.1: 1-17 (2021).
24. Lin, S., Werle, J. & Korb, J. Transcriptomic analyses of the termite, *Cryptotermes secundus*, reveal a gene network underlying a long lifespan and high fecundity. *Communications Biology* **4**, 1–12 (2021).
25. Haroon *et al.* Transcriptomic evidence that insulin signalling pathway regulates the ageing of subterranean termite castes. *Scientific Reports* **10**, 8187 (2020).
26. Harrison, M. C. *et al.* Gene co-expression network reveals highly conserved, well-regulated anti-ageing mechanisms in old ant queens. *Genome Biology and Evolution* (2021).
27. Negroni, M. A., Foitzik, S. & Feldmeyer, B. Long-lived *Temnothorax* ant queens switch from investment in immunity to antioxidant production with age. *Scientific Reports* **9**, 7270 (2019).
28. Fontana, L. & Partridge, L. Promoting health and longevity through diet: from model organisms to humans. *Cell* **161**, 106–118 (2015).
29. Álvarez-Rendón, J. P., Salceda, R. & Riesgo-Escovar, J. R. *Drosophila melanogaster* as a model for diabetes type 2 progression. *BioMed Research International* vol. 2018.
30. Arrese, E. L. & Soulages, J. L. Insect fat body: energy, metabolism, and regulation. *Annual Review Entomol*ogy **55**, 207–225 (2009).
31. Li, S., Yu, X. & Feng, Q. Fat body biology in the last decade. *Annual Review of Entomology* **64**, 315–333 (2019).
32. Giannakou, M. E. *et al.* Long-lived *Drosophila* with overexpressed dFOXO in adult fat body. *Science* **305**, 361–361 (2004).
33. Bjedov, I. *et al.* Mechanisms of life span extension by rapamycin in the fruit fly *Drosophila melanogaster*. *Cell Metabolism* **11**, 35–46 (2010).
34. Partridge, L., Alic, N., Bjedov, I. & Piper, M. D. W. Ageing in *Drosophila*: the role of the insulin/Igf and TOR signalling network. *Experimental Gerontology* **46**, 376–381 (2011).
35. Roisin, Y. Diversity and evolution of caste patterns. in *Termites: Evolution, Sociality, Symbioses, Ecology* (eds. Abe, T., Bignell, D. E. & Higashi, M.) 95–119 (Springer Netherlands, 2000).
36. Lepage, M. Development in the laboratory of incipient colonies of *Macrotermes michaelseni* (Sjoestedt) (Isoptera, Macrotermitidae). *Annales de la Societe Entomologique de France* (1990).
37. Langfelder, P. & Horvath, S. WGCNA: an R package for weighted correlation network analysis. *BMC Bioinformatics* **9**, 559 (2008).
38. Brina, D. *et al.* eIF6 coordinates insulin sensitivity and lipid metabolism by coupling

translation to transcription. *Nature Communications* **6**, 8261 (2015).
39. Buszczak, M., Lu, X., Segraves, W. A., Chang, T. Y. & Cooley, L. Mutations in the midway gene disrupt a drosophila acyl coenzyme A: diacylglycerol acyltransferase. *Genetics* **160**, 1511–1518 (2002).
40. Han, S. H. & Bordereau, C. Origin and formation of the royal fat body of the higher termite queens. *Journal of Morphology* **173**, 17–28 (1982).
41. Nozaki, T. & Matsuura, K. Evolutionary relationship of fat body endoreduplication and queen fecundity in termites. *Ecology and Evolution* **9**, 11684–11694 (2019).
42. Herzig, S. & Shaw, R. J. AMPK: guardian of metabolism and mitochondrial homeostasis. *Nature Reviews Molecular Cell Biology* **19**, 121–135 (2018).
43. Jeon, S.-M. Regulation and function of AMPK in physiology and diseases. *Experimental and Molecular Medecine* **48**, e245 (2016).
44. Thompson, S. N.. Trehalose—the insect 'blood'sugar. Advances in insect physiology, Vol 31, 205-285. (Elsevier, 2003).
45. Gems, D. & Partridge, L. Genetics of longevity in model organisms: debates and paradigm Shifts. *Annual Revview of Physiology* **75**, 621–644 (2013).
46. Lee, D., Son, H. G., Jung, Y. & Lee, S.-J. V. The role of dietary carbohydrates in organismal aging. *Cellular and Molecular Life Sciences* **74**, 1793–1803 (2017).
47. Musselman, L. P. *et al.* A high-sugar diet produces obesity and insulin resistance in wild-type *Drosophila*. *Disease Models & Mechanisms* **4**, 842–849 (2011).
48. Wang, Y., Viscarra, J., Kim, S.-J. & Sul, H. S. Transcriptional regulation of hepatic lipogenesis. *Nature Reviews Molecular Cell Biology* **16**, 678–689 (2015).
49. Poulsen, M. *et al.* Complementary symbiont contributions to plant decomposition in a fungus-farming termite. *PNAS* **111**, 14500–14505 (2014).
50. Pagliassotti, M. J. *et al.* Trehalose supplementation reduces hepatic endoplasmic reticulum stress and inflammatory signaling in old mice. *The Journal of Nutritional Biochemistry* **45**, 15–23 (2017).
51. Honda, Y., Tanaka, M. & Honda, S. Trehalose extends longevity in the nematode *Caenorhabditis elegans*. *Aging Cell* **9**, 558–569 (2010).
52. Seo, Y., Kingsley, S., Walker, G., Mondoux, M. A. & Tissenbaum, H. A. Metabolic shift from glycogen to trehalose promotes lifespan and healthspan in *Caenorhabditis elegans*. *PNAS* **115**, E2791–E2800 (2018).
53. Miwa, S., Lawless, C. & Zglinicki, T. V. Mitochondrial turnover in liver is fast in vivo and is accelerated by dietary restriction: application of a simple dynamic model. *Aging Cell* **7**, 920–923 (2008).
54. Guarente, L. Mitochondria—A Nexus for aging, calorie restriction, and sirtuins? *Cell* **132**, 171–176 (2008).
55. López-Lluch, G. *et al.* Calorie restriction induces mitochondrial biogenesis and bioenergetic efficiency. *PNAS* **103**, 1768–1773 (2006).
56. López-Lluch, G. & Navas, P. Calorie restriction as an intervention in ageing. *The Journal of Physiology* **594**, 2043–2060 (2016).
57. Gilbert, L. I. & Chino, H. Transport of lipids in insects. *J. Lipid Res.* **15**, 439–456 (1974).
58. Slaidina, M., Delanoue, R., Gronke, S., Partridge, L. & Léopold, P. A drosophila insulin-like peptide promotes growth during nonfeeding states. *Developmental Cell* **17**, 874–884 (2009).
59. Bai, H., Kang, P. & Tatar, M. drosophila insulin-like peptide-6 (dilp6) expression from fat body extends lifespan and represses secretion of drosophila insulin-like peptide-2 from the brain. *Aging Cell* **11**, 978–985 (2012).
60. Miluzio, A. *et al.* Translational control by mTOR-independent routes: how eIF6 organizes metabolism. *Biochemical Society Transactions* **44**, 1667–1673 (2016).

61. Wang, X. & Proud, C. G. Nutrient control of TORC1, a cell-cycle regulator. *Trends in Cell Biology* **19**, 260–267 (2009).
62. Ristow, M. & Schmeisser, K. Mitohormesis: Promoting health and lifespan by increased levels of reactive oxygen species (ROS). *Dose-Response* **12**, dose-response.13-035.Ristow (2014).
63. Palmeira, C. M. *et al.* Mitohormesis and metabolic health: The interplay between ROS, cAMP and sirtuins. *Free Radical Biology and Medicine* **141**, 483–491 (2019).
64. Bárcena, C., Mayoral, P. & Quirós, P. M. Chapter Two - Mitohormesis, an antiaging paradigm. in *International Review of Cell and Molecular Biology* (eds. López-Otín, C. & Galluzzi, L.) vol. 340 35–77 (Academic Press, 2018).
65. Corona, M., Hughes, K. A., Weaver, D. B. & Robinson, G. E. Gene expression patterns associated with queen honey bee longevity. *Mechanisms of Ageing and Development* **126**, 1230–1238 (2005).
66. Parker, J. D., Parker, K. M., Sohal, B. H., Sohal, R. S. & Keller, L. Decreased expression of Cu–Zn superoxide dismutase 1 in ants with extreme lifespan. *PNAS* **101**, 3486–3489 (2004).
67. Martin, N. *et al.* Honey bee caste lipidomics in relation to life-history stage and the long life of the queen. *Journal of Experimental Biology* **222**, (2019).
68. Munro, D. & Blier, P. U. The extreme longevity of *Arctica islandica* is associated with increased peroxidation resistance in mitochondrial membranes. *Aging Cell* **11**, 845–855 (2012).
69. Uys, V. M. & Plant Protection Research Institute (South Africa). *A guide to the termite genera of Southern Africa*. (Plant Protection Research Institute, Agricultural Research Council, 2002).
70. Mitchell, J. D. Colony foundation and the development of incipient laboratory colonies of *Macrotermes natalensis* (Haviland) (Termitidae: Macrotermitinae). African Entomology **28**, 215–224 (2020).
71. Sillam-Dussès, D. *Trail pheromones and sex pheromones in termites*. (Nova Science Publishers/Novinka, 2010).
72. Licht, H. H. D. F., Boomsma, J. J. & Aanen, D. K. Presumptive horizontal symbiont transmission in the fungus-growing termite *Macrotermes natalensis*. *Molecular Ecology* **15**, 3131–3138 (2006).
73. Folmer, O., Black, M., Hoeh, W., Lutz, R. & Vrijenhoek, R. DNA primers for amplification of mitochondrial cytochrome c oxidase subunit 1 from diverse metazoan invertebrates. *Molecular Marine Biology and Biotechnology* (1994).
74. Kim, D., Paggi, J. M., Park, C., Bennett, C. & Salzberg, S. L. Graph-based genome alignment and genotyping with HISAT2 and HISAT-genotype. *Nature Biotechnology* **37**, 907–915 (2019).
75. Anders, S., Pyl, P. T. & Huber, W. HTSeq—a Python framework to work with high-throughput sequencing data. *Bioinformatics* **31**, 166–169 (2015).
76. Love, M. I., Huber, W. & Anders, S. Moderated estimation of fold change and dispersion for RNA-seq data with DESeq2. *Genome Biology* **15**, 550 (2014).
77. Shannon, P. *et al.* Cytoscape: A software environment for integrated models of biomolecular interaction networks. *Genome Research* **13**, 2498–2504 (2003).
78. Alexa, A. & Rahnenfuhrer, J. topGO: Enrichment analysis for Gene Ontology. R package version 2.28. 0. *BioConductor. Published online* (2016).
79. Rivera, M. C., Jain, R., Moore, J. E. & Lake, J. A. Genomic evidence for two functionally distinct gene classes. *PNAS* **95**, 6239–6244 (1998).
80. Camacho C, et al. Blast+: architecture and applications. BMC Bioinformatics. 10(1):421(2009).

911 81. Slater, G. S. C. & Birney, E. Automated generation of heuristics for biological sequence
912 comparison. *BMC Bioinformatics* **6**, 31 (2005).
913 82. Notredame, C., Higgins, D. G. & Heringa, J. T-coffee: a novel method for fast and
914 accurate multiple sequence alignment Edited by J. Thornton. *Journal of Molecular*
915 *Biology* **302**, 205–217 (2000).
916 83. Capella-Gutiérrez, S., Silla-Martínez, J. M. & Gabaldón, T. trimAl: a tool for automated
917 alignment trimming in large-scale phylogenetic analyses. *Bioinformatics* **25**, 1972–1973
918 (2009).
919 84. Minh, B. Q. *et al.* IQ-TREE 2: New models and efficient methods for phylogenetic
920 inference in the genomic Era. *Molecular Biology and Evolution* **37**, 1530–1534 (2020).
921 85. Letunic, I. & Bork, P. Interactive Tree Of Life (iTOL) v5: an online tool for phylogenetic
922 tree display and annotation. *Nucleic Acids Research* **49**, W293–W296 (2021).
923 86. Khodayari, S., Moharramipour, S., Larvor, V., Hidalgo, K. & Renault, D. Deciphering
924 the metabolic changes associated with diapause syndrome and cold acclimation in the
925 two-spotted spider mite *Tetranychus urticae*. *PLOS ONE* **8**, e54025 (2013).
926 87. Genitoni, J. *et al.* Hypomethylation of the aquatic invasive plant, *Ludwigia grandiflora*
927 subsp. *hexapetala* mimics the adaptive transition into the terrestrial morphotype.
928 *Physiologia Plantarum* **170**, 280–298 (2020).
929 88. McArdle, B. H. & Anderson, M. J. Fitting multivariate models to community data: A
930 comment on distance-based redundancy analysis. *Ecology* **82**, 290–297 (2001).
931 89. Cajka, T., Smilowitz, J. T. & Fiehn, O. Validating quantitative untargeted lipidomics
932 across nine liquid chromatography–high-resolution mass spectrometry platforms.
933 *Analytical Chemistry.* **89**, 12360–12368 (2017).
934 90. Merlier, F., Imatoukene, N., Octave, S., Nicaud, J.-M. & Thomasset, B. A gas
935 chromatography full scan high resolution Orbitrap mass spectrometry method for
936 separation and characterization of 3-hydroxymethyl pyridine ester of fatty acids at low
937 levels. *Journal of Chromatography A* **1575**, 72–79 (2018).
938 91. Ulmer, C. Z., Patterson, R. E., Koelmel, J. P., Garrett, T. J. & Yost, R. A. A Robust
939 Lipidomics workflow for mammalian cells, plasma, and tissue using liquid-
940 chromatography high-resolution tandem mass spectrometry. in *Lipidomics: Methods*
941 *and Protocols* (ed. Bhattacharya, S. K.) 91–106 (Springer, 2017).
942 92. Tsugawa, H. *et al.* A lipidome atlas in MS-DIAL 4. *Nature Biotechnology* **38**, 1159–
943 1163 (2020).
944 93. Van den Boogaart, K. G., & Tolosana-Delgado, R. Analyzing compositional data with
945 R Vol. 122 (Heidelberg: Springer 2013).

946 **FIGURE LEGENDS**

947 **Figure 1: Overview of the model system.** Timeline of the different stages of *Macrotermes natalensis*
948 colonies founded from one male and one female imago each (T0). Queens from incipient laboratory
949 colonies were sampled at 3 months after colony establishment (QT1), 9 months (QT2) and 31 months
950 (QT3). Field termite colonies over 20 years old are added. From field colonies, queens (QT0 and
951 QT4), workers (FW) and kings (KT4) were sampled. Wild oats were supplied to the laboratory
952 colonies from 3 months onward and the fungus *Termitomyces* sp. was introduced artificially in 3.5
953 months old colonies. Wood was supplied from 4.5 months onward. The drawings represent winged
954 imagoes, workers, kings and queens at the different stages (physogastric queens become larger).
955 Replication and sampling in our incipient colonies are further described in Supplementary Table 1.

956 **Figure 2: Weighted Gene Co-expression Network Analysis (WGCNA).** The gene co-expression
957 network is displayed with genes as nodes and edges representing the co-expression relationships
958 between genes. Nine modules were detected within which gene expression was especially strongly
959 correlated (see Supplementary Fig. 2 for more details.) Shown are the seven largest modules,
960 represented by colours. For each module, information is supplied on the caste or queen stage with
961 which module expression is significantly correlated; upward arrow indicates a significant increase,
962 downward arrow a significant decrease, in expression. The top 3 enriched GO-terms associated with
963 the gene members of each module are displayed (for full lists of significant GO-terms see
964 supplementary Table 2). This network was created with Cytoscape (version 3.8.0; Shannon et al 2003)
965 on a reduced representation of the WGCN containing the top connected genes (see methods for more
966 details).

967 **Figure 3: Caste related changes in gene expression.** Heatmap representing standardized gene
968 expression (blue = low; red = high) in fat bodies of FW, QT4 and KT4. Annotations to the right of
969 the heatmap include WGCN module (Supplementary Fig. 2), gene names and gene acronyms in

970 *Drosophila melanogaster* (*D. melanogaster*) and *Homo sapiens* (*H. sapiens*). The map is restricted
971 to expression of genes involved in metabolic signaling, lipid metabolism, mitochondrial oxidative
972 phosphorylation system (OXPHOS), mitochondrial ribosome proteins, mitochondrial fission,
973 mitochondrial transport, antioxidant defense and DNA repair. Expression of all genes differ
974 significantly between FW versus QT4 and between FW versus KT4. The number of replicates per
975 group is provided in Supplementary Table 1.

976 **Figure 4: Phylogenetic tree of ILP genes in several insect species.** The two ILPs found in the M.
977 natalensis genome (*Ilp7* = Mnat03820c and *Ilp9* = Mnat00258c) are highlighted in red and the 8
978 Drosophila genes (*DILPs*) are highlighted in blue. All other species can be identified by their GeneID
979 displayed in the Table. New annotations and protein sequences are available at
980 github.com/MCH74/Mnat_analyses). The tree was constructed with iqtree2 (Q.pfam+R4 model and
981 10,000 bootstraps) and visualized with iTOL (v. 6). Branch labels are bootstraps, the tree is rooted at
982 the Strigamia maritima gene.

983 **Figure 5: Heatmap with the expression of genes in fat bodies during adult queen maturation**
984 **involved in lipid metabolism.** Heatmap representing standardized gene expression (blue = low; red
985 = high) at each of the five queen stages (QT0-QT4). Annotations to the right of the heatmap include
986 WGCN module (Supplementary Fig. 2), gene name and gene acronyms in *Drosophila melanogaster*
987 (*D. melanogaster*) and *Homo sapiens* (*H. sapiens*). Number of replicates per group is provided in
988 Supplementary Table 1. Greater than or less than symbols (>/<) represent significant differences in
989 expression.

990 **Figure 6: Canonical discriminant analysis of concentrations of metabolites**. Three canonical
991 functions discriminate ages and castes significantly, of which we show scores for the first two.
992 Average scores for each caste and age are shown, plus canonical structure coefficients of each
993 metabolite as vectors from the origin. These are proportional in length to the magnitudes of the

correlations of each metabolite with the scores of the discriminant functions and show how information from each metabolite aids in discriminating castes and ages. Numbers of replicates per group are provided in Supplementary Table 1.

Figure 7: Comparison of lipid profiles between FW and QT4 in hemolymph. Hierarchical clustering heatmap analysis of triglycerides (TG, orange), diglycerides (DG, green), phosphatidylethanolamine (PE, black), phosphatidylcholine (PC, grey), lysophosphatidylcholine (LPC, yellow), sphingomyelin (SM, blue) lipids in hemolymph of FW and QT4 performed in MetaboAnalyst 4.0. Individual lipids are shown in rows and samples displayed in columns, according to cluster analysis (Euclidian distance was used and Ward's clustering algorithm). The colour gradient, ranging from dark blue through white to dark red, represents low, middle and high abundance of a lipid. Numbers of replicates per group are provided in Supplementary Table 1.

Figure 8: Changes in lipid profiles in fat bodies during adult queen maturation. (a) Hierarchical clustering heatmap analysis of triglycerides (TG, orange), diglycerides (DG, green), phosphatidylethanolamine (PE, black), phosphatidylcholine (PC, grey), lysophosphatidylcholine (LPC, yellow), sphingomyelin (SM, blue) lipids in fat body of different stage of queen (QT0, QT2 and QT4) performed in MetaboAnalyst 4.0. Individual lipids are shown per row and mean of lipid amount of each stage displayed in columns, according to cluster analysis (Euclidean distance and Ward's algorithm). The colour gradient, ranging from dark blue through white to dark red, represents low, middle and high abundance of a given lipid **(b)** Percentages (%) of saturated fatty acids (SFA), monounsaturated fatty acids (MUFA) and polyunsaturated fatty acids (PUFA) of total FA in fat bodies of of different queen maturation stages (QT0, QT2, QT4). Ternary graph showing the percentages of SFA (orange), MUFA (black) and PUFA (blue). The table below shows the averages of MUFA, SFA and PUFA for each stage. Permutational MANOVA demonstrated that SFA/MUFA/PUFA proportions in fat bodies of QT2 and QT4 were significantly different relative to QT0 (Permutational MANOVA, p-value = 0.012). **(c)** Box plot illustrating the peroxidation index of

1019 fat bodies of different queen maturation stages (QT0, QT2 and QT4). A box consists of upper and
1020 lower hinges and a center line corresponding to the 25th percentile, the 75th percentile and the
1021 median, respectively. Rhombuses represent the averages. Different letters indicate significantly
1022 different values according to a Kruskal-Wallis test followed by pairwise Dunn tests (p-values < 0.05).
1023 The number of replicates per group is provided in Supplementary Table 1.

1024

1025

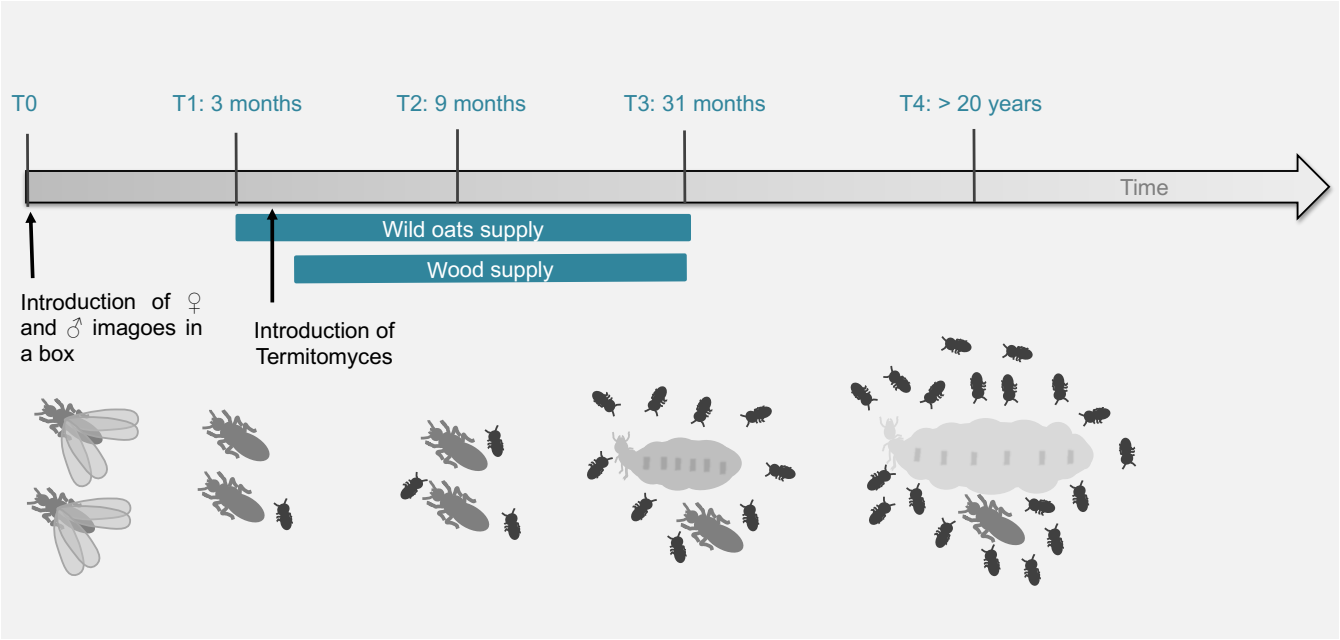
T0
T1: 3 months
T2: 9 months
T3: 31 months
T4: > 20 years
Time
Wild oats supply
Wood supply
Introduction of ♀ and ♂ imagoes in a box
Introduction of Termitomyces

Figure 1

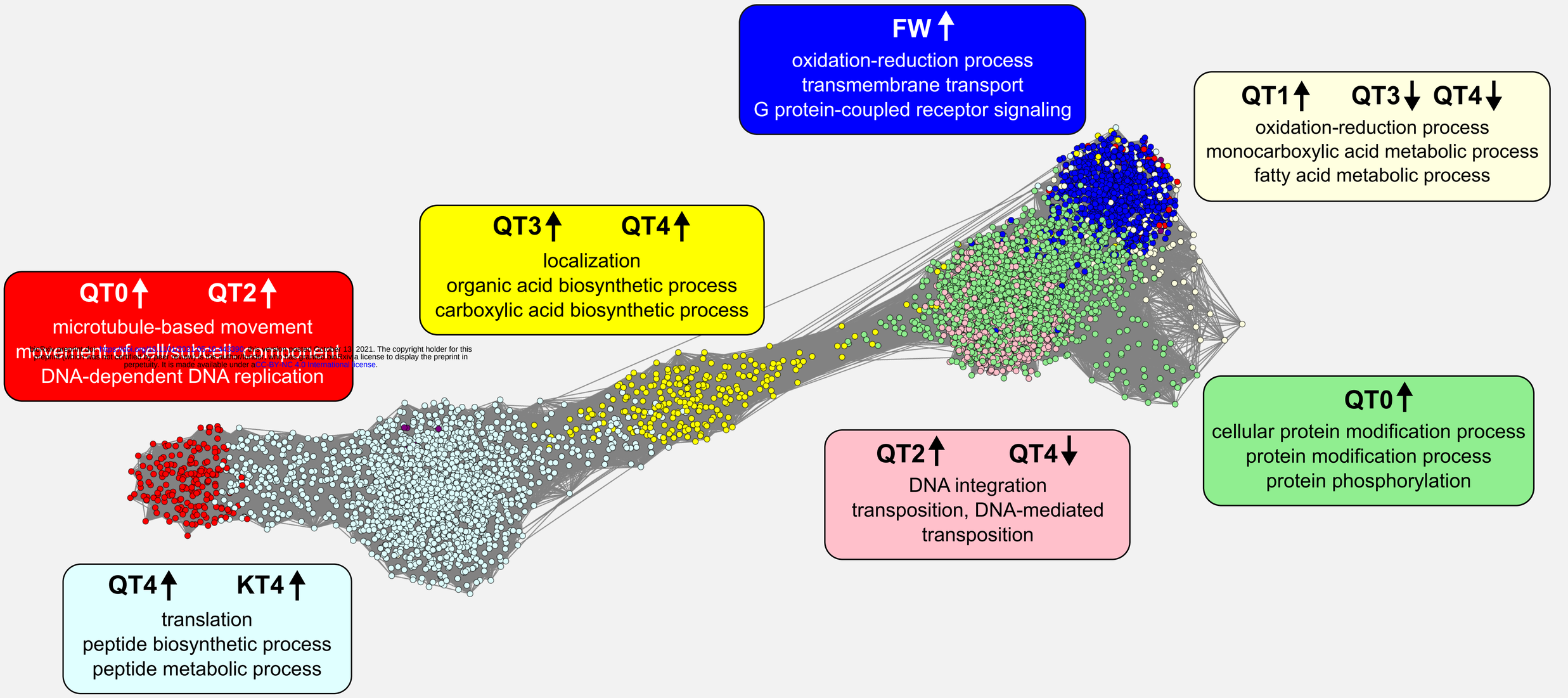

Figure 2

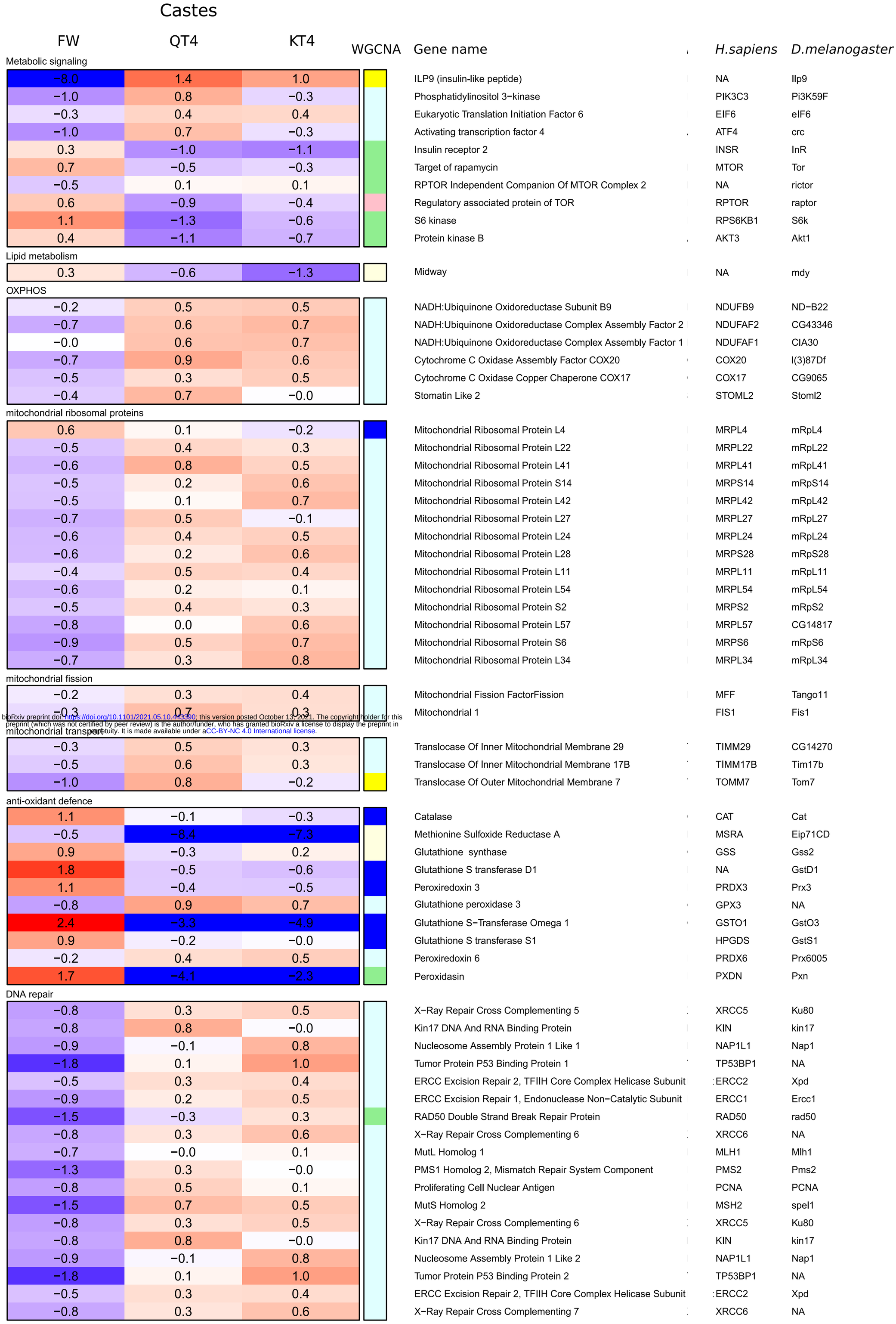

Figure 3

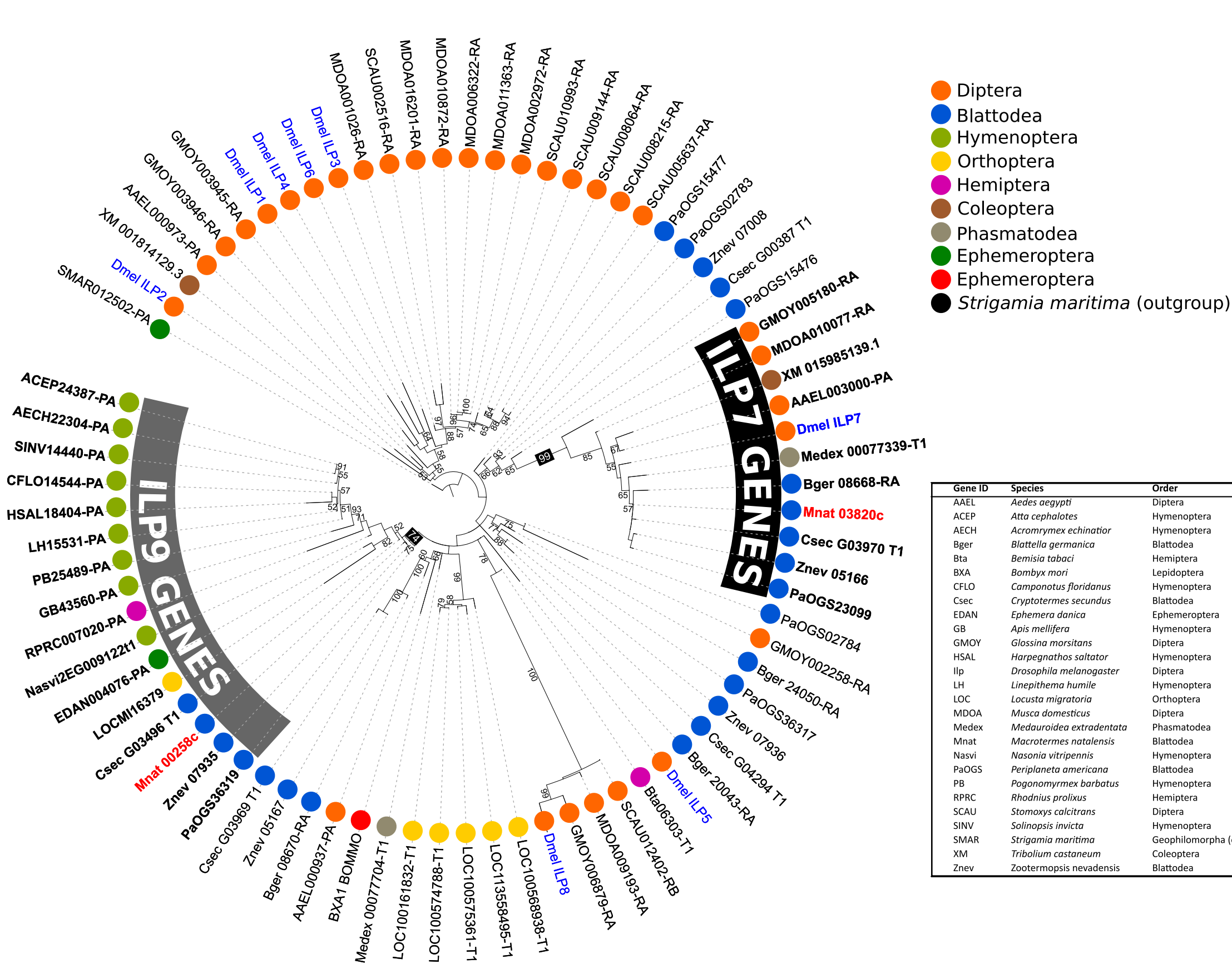

Gene ID	Species	Order
AAEL	*Aedes aegypti*	Diptera
ACEP	*Atta cephalotes*	Hymenoptera
AECH	*Acromrymex echinatior*	Hymenoptera
Bger	*Blattella germanica*	Blattodea
Bta	*Bemisia tabaci*	Hemiptera
BXA	*Bombyx mori*	Lepidoptera
CFLO	*Camponotus floridanus*	Hymenoptera
Csec	*Cryptotermes secundus*	Blattodea
EDAN	*Ephemera danica*	Ephemeroptera
GB	*Apis mellifera*	Hymenoptera
GMOY	*Glossina morsitans*	Diptera
HSAL	*Harpegnathos saltator*	Hymenoptera
Ilp	*Drosophila melanogaster*	Diptera
LH	*Linepithema humile*	Hymenoptera
LOC	*Locusta migratoria*	Orthoptera
MDOA	*Musca domesticus*	Diptera
Medex	*Medauroidea extradentata*	Phasmatodea
Mnat	*Macrotermes natalensis*	Blattodea
Nasvi	*Nasonia vitripennis*	Hymenoptera
PaOGS	*Periplaneta americana*	Blattodea
PB	*Pogonomyrmex barbatus*	Hymenoptera
RPRC	*Rhodnius prolixus*	Hemiptera
SCAU	*Stomoxys calcitrans*	Diptera
SINV	*Solinopsis invicta*	Hymenoptera
SMAR	*Strigamia maritima*	Geophilomorpha (outgroup)
XM	*Tribolium castaneum*	Coleoptera
Znev	Zootermopsis nevadensis	Blattodea

Figure 4

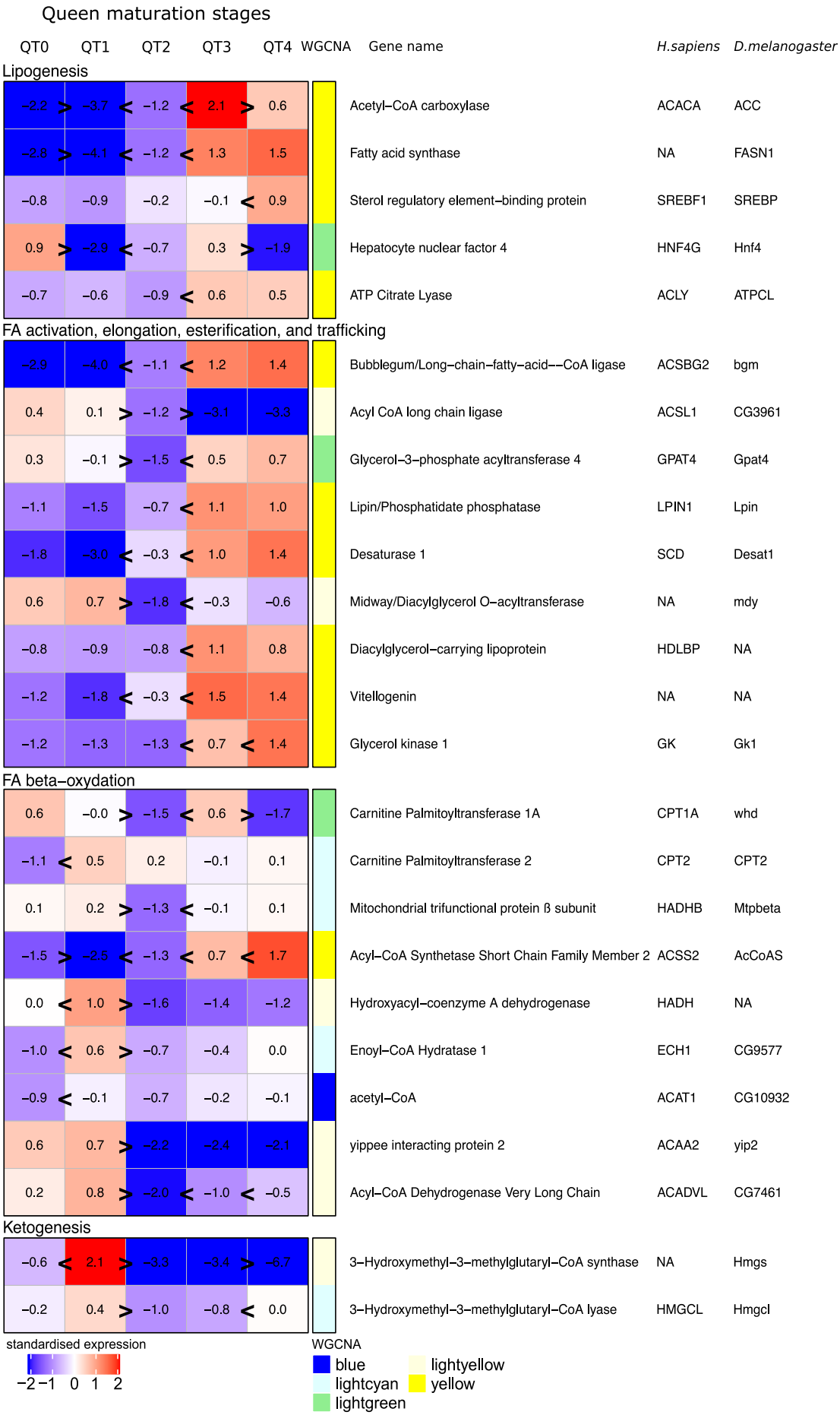
Queen maturation stages
QT0
QT1
QT2
QT3
QT4
WGCNA
Gene name
H.sapiens
D.melanogaster
Lipogenesis
−2.2 −3.7 −1.2 2.1 0.6 Acetyl−CoA carboxylase ACACA ACC
−2.8 −4.1 −1.2 1.3 1.5 Fatty acid synthase NA FASN1
−0.8 −0.9 −0.2 −0.1 0.9 Sterol regulatory element−binding protein SREBF1 SREBP
0.9 −2.9 −0.7 0.3 −1.9 Hepatocyte nuclear factor 4 HNF4G Hnf4
−0.7 −0.6 −0.9 0.6 0.5 ATP Citrate Lyase ACLY ATPCL
FA activation, elongation, esterification, and trafficking
−2.9 −4.0 −1.1 1.2 1.4 Bubblegum/Long−chain−fatty−acid−−CoA ligase ACSBG2 bgm
0.4 0.1 −1.2 −3.1 −3.3 Acyl CoA long chain ligase ACSL1 CG3961
0.3 −0.1 −1.5 0.5 0.7 Glycerol−3−phosphate acyltransferase 4 GPAT4 Gpat4
−1.1 −1.5 −0.7 1.1 1.0 Lipin/Phosphatidate phosphatase LPIN1 Lpin
−1.8 −3.0 −0.3 1.0 1.4 Desaturase 1 SCD Desat1
0.6 0.7 −1.8 −0.3 −0.6 Midway/Diacylglycerol O−acyltransferase NA mdy
−0.8 −0.9 −0.8 1.1 0.8 Diacylglycerol−carrying lipoprotein HDLBP NA
−1.2 −1.8 −0.3 1.5 1.4 Vitellogenin NA NA
−1.2 −1.3 −1.3 0.7 1.4 Glycerol kinase 1 GK Gk1
FA beta−oxydation
0.6 −0.0 −1.5 0.6 −1.7 Carnitine Palmitoyltransferase 1A CPT1A whd
−1.1 0.5 0.2 −0.1 0.1 Carnitine Palmitoyltransferase 2 CPT2 CPT2
0.1 0.2 −1.3 −0.1 0.1 Mitochondrial trifunctional protein ß subunit HADHB Mtpbeta
−1.5 −2.5 −1.3 0.7 1.7 Acyl−CoA Synthetase Short Chain Family Member 2 ACSS2 AcCoAS
0.0 1.0 −1.6 −1.4 −1.2 Hydroxyacyl−coenzyme A dehydrogenase HADH NA
−1.0 0.6 −0.7 −0.4 0.0 Enoyl−CoA Hydratase 1 ECH1 CG9577
−0.9 −0.1 −0.7 −0.2 −0.1 acetyl−CoA ACAT1 CG10932
0.6 0.7 −2.2 −2.4 −2.1 yippee interacting protein 2 ACAA2 yip2
0.2 0.8 −2.0 −1.0 −0.5 Acyl−CoA Dehydrogenase Very Long Chain ACADVL CG7461
Ketogenesis
−0.6 2.1 −3.3 −3.4 −6.7 3−Hydroxymethyl−3−methylglutaryl−CoA synthase NA Hmgs
−0.2 0.4 −1.0 −0.8 0.0 3−Hydroxymethyl−3−methylglutaryl−CoA lyase HMGCL Hmgcl
standardised expression
−2 −1 0 1 2
WGCNA
blue
lightcyan
lightgreen
lightyellow
yellow

Figure 5

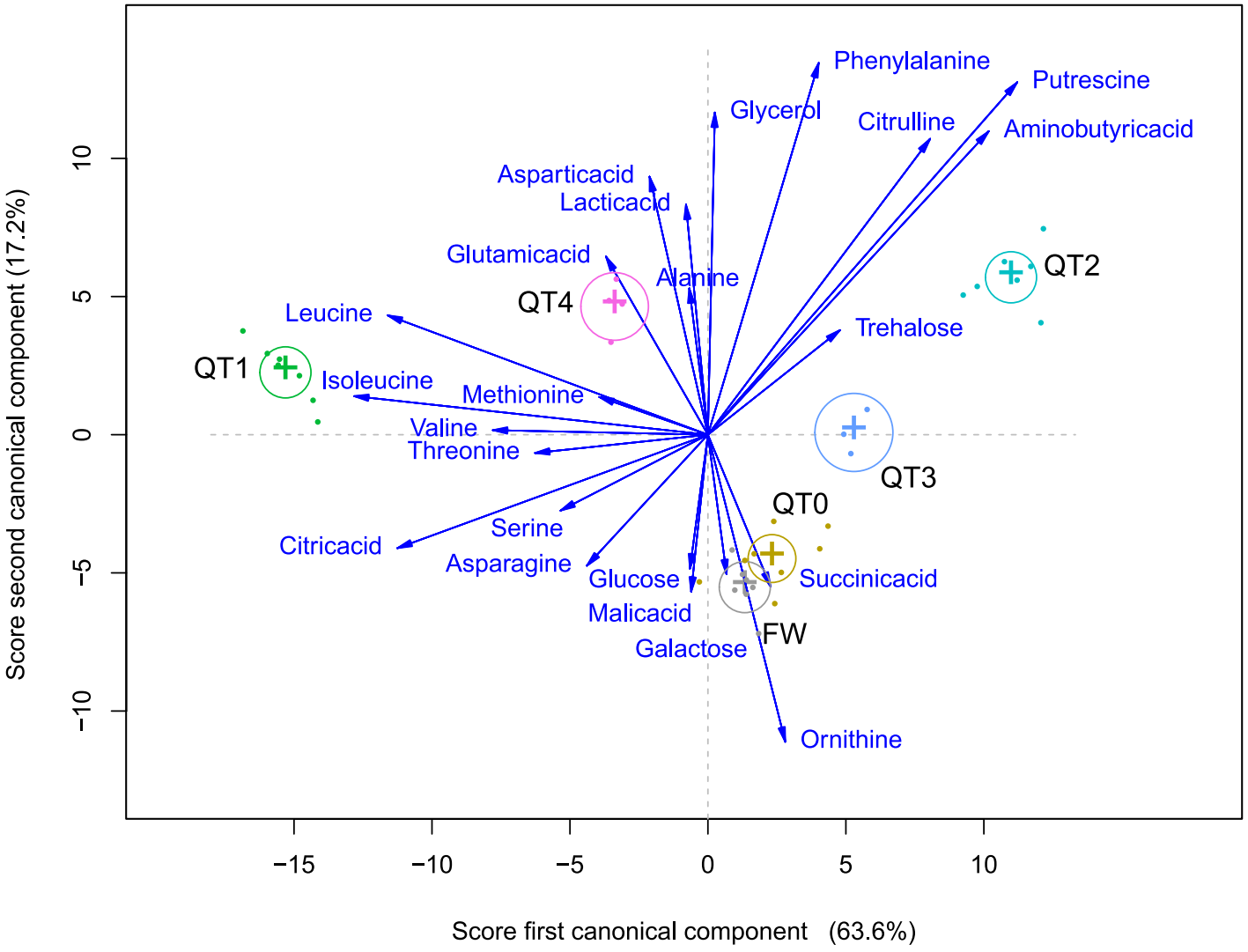
Phenylalanine
Putrescine
Glycerol
Citrulline
Aminobutyricacid
Asparticacid
Lacticacid
Glutamicacid
Alanine
QT4
QT2
Leucine
Trehalose
QT1
Isoleucine
Methionine
Valine
Threonine
QT3
QT0
Serine
Citricacid
Asparagine
Glucose
Succinicacid
Malicacid
FW
Galactose
Ornithine
Score second canonical component (17.2%)
10
5
0
−5
−10
−15
−10
−5
0
5
10
Score first canonical component (63.6%)

Figure 6

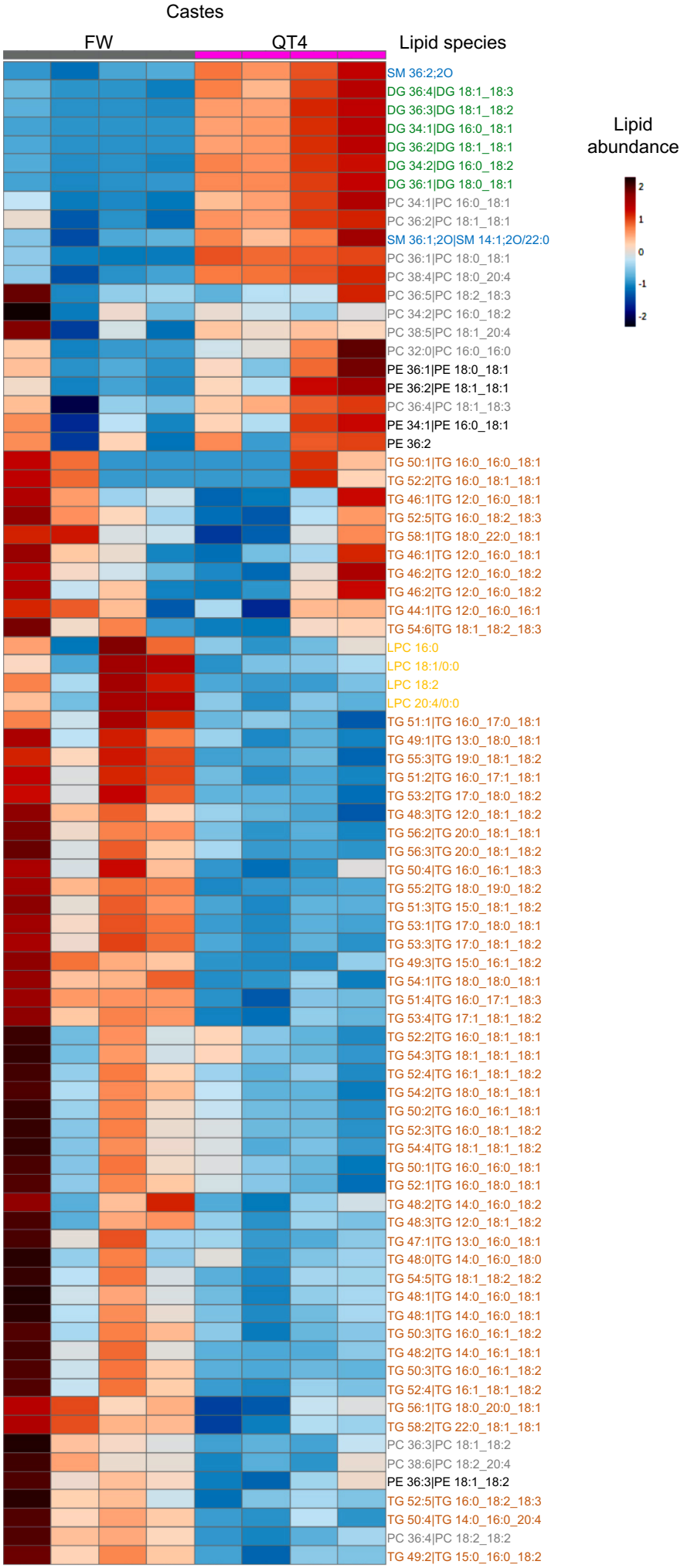
Castes
FW
QT4
Lipid species
Lipid abundance
2
1
0
-1
-2
SM 36:2;2O
DG 36:4|DG 18:1_18:3
DG 36:3|DG 18:1_18:2
DG 34:1|DG 16:0_18:1
DG 36:2|DG 18:1_18:1
DG 34:2|DG 16:0_18:2
DG 36:1|DG 18:0_18:1
PC 34:1|PC 16:0_18:1
PC 36:2|PC 18:1_18:1
SM 36:1;2O|SM 14:1;2O/22:0
PC 36:1|PC 18:0_18:1
PC 38:4|PC 18:0_20:4
PC 36:5|PC 18:2_18:3
PC 34:2|PC 16:0_18:2
PC 38:5|PC 18:1_20:4
PC 32:0|PC 16:0_16:0
PE 36:1|PE 18:0_18:1
PE 36:2|PE 18:1_18:1
PC 36:4|PC 18:1_18:3
PE 34:1|PE 16:0_18:1
PE 36:2
TG 50:1|TG 16:0_16:0_18:1
TG 52:2|TG 16:0_18:1_18:1
TG 46:1|TG 12:0_16:0_18:1
TG 52:5|TG 16:0_18:2_18:3
TG 58:1|TG 18:0_22:0_18:1
TG 46:1|TG 12:0_16:0_18:1
TG 46:2|TG 12:0_16:0_18:2
TG 46:2|TG 12:0_16:0_18:2
TG 44:1|TG 12:0_16:0_16:1
TG 54:6|TG 18:1_18:2_18:3
LPC 16:0
LPC 18:1/0:0
LPC 18:2
LPC 20:4/0:0
TG 51:1|TG 16:0_17:0_18:1
TG 49:1|TG 13:0_18:0_18:1
TG 55:3|TG 19:0_18:1_18:2
TG 51:2|TG 16:0_17:1_18:1
TG 53:2|TG 17:0_18:0_18:2
TG 48:3|TG 12:0_18:1_18:2
TG 56:2|TG 20:0_18:1_18:1
TG 56:3|TG 20:0_18:1_18:2
TG 50:4|TG 16:0_16:1_18:3
TG 55:2|TG 18:0_19:0_18:2
TG 51:3|TG 15:0_18:1_18:2
TG 53:1|TG 17:0_18:0_18:1
TG 53:3|TG 17:0_18:1_18:2
TG 49:3|TG 15:0_16:1_18:2
TG 54:1|TG 18:0_18:0_18:1
TG 51:4|TG 16:0_17:1_18:3
TG 53:4|TG 17:1_18:1_18:2
TG 52:2|TG 16:0_18:1_18:1
TG 54:3|TG 18:1_18:1_18:1
TG 52:4|TG 16:1_18:1_18:2
TG 54:2|TG 18:0_18:1_18:1
TG 50:2|TG 16:0_16:1_18:1
TG 52:3|TG 16:0_18:1_18:2
TG 54:4|TG 18:1_18:1_18:2
TG 50:1|TG 16:0_16:0_18:1
TG 52:1|TG 16:0_18:0_18:1
TG 48:2|TG 14:0_16:0_18:2
TG 48:3|TG 12:0_18:1_18:2
TG 47:1|TG 13:0_16:0_18:1
TG 48:0|TG 14:0_16:0_18:0
TG 54:5|TG 18:1_18:2_18:2
TG 48:1|TG 14:0_16:0_18:1
TG 48:1|TG 14:0_16:0_18:1
TG 50:3|TG 16:0_16:1_18:2
TG 48:2|TG 14:0_16:1_18:1
TG 50:3|TG 16:0_16:1_18:2
TG 52:4|TG 16:1_18:1_18:2
TG 56:1|TG 18:0_20:0_18:1
TG 58:2|TG 22:0_18:1_18:1
PC 36:3|PC 18:1_18:2
PC 38:6|PC 18:2_20:4
PE 36:3|PE 18:1_18:2
TG 52:5|TG 16:0_18:2_18:3
TG 50:4|TG 14:0_16:0_20:4
PC 36:4|PC 18:2_18:2
TG 49:2|TG 15:0_16:0_18:2

Figure 7

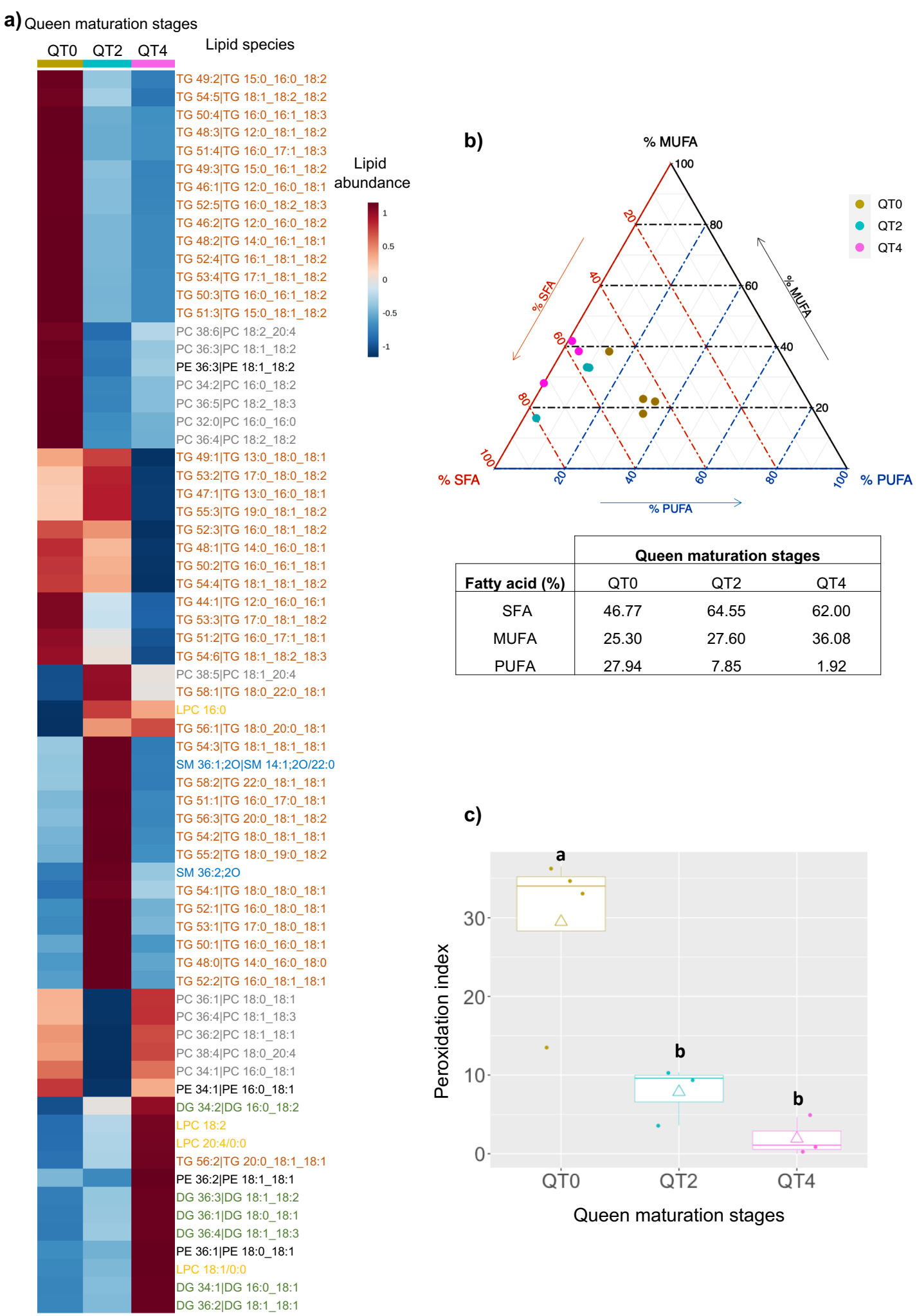

	Queen maturation stages		
Fatty acid (%)	QT0	QT2	QT4
SFA	46.77	64.55	62.00
MUFA	25.30	27.60	36.08
PUFA	27.94	7.85	1.92

Figure 8